Chapter 6

A Study on Structure and Dynamics of modified ASO/RNA hybrid gapmer type duplexes in complex with Human RNase H catalytic domain.

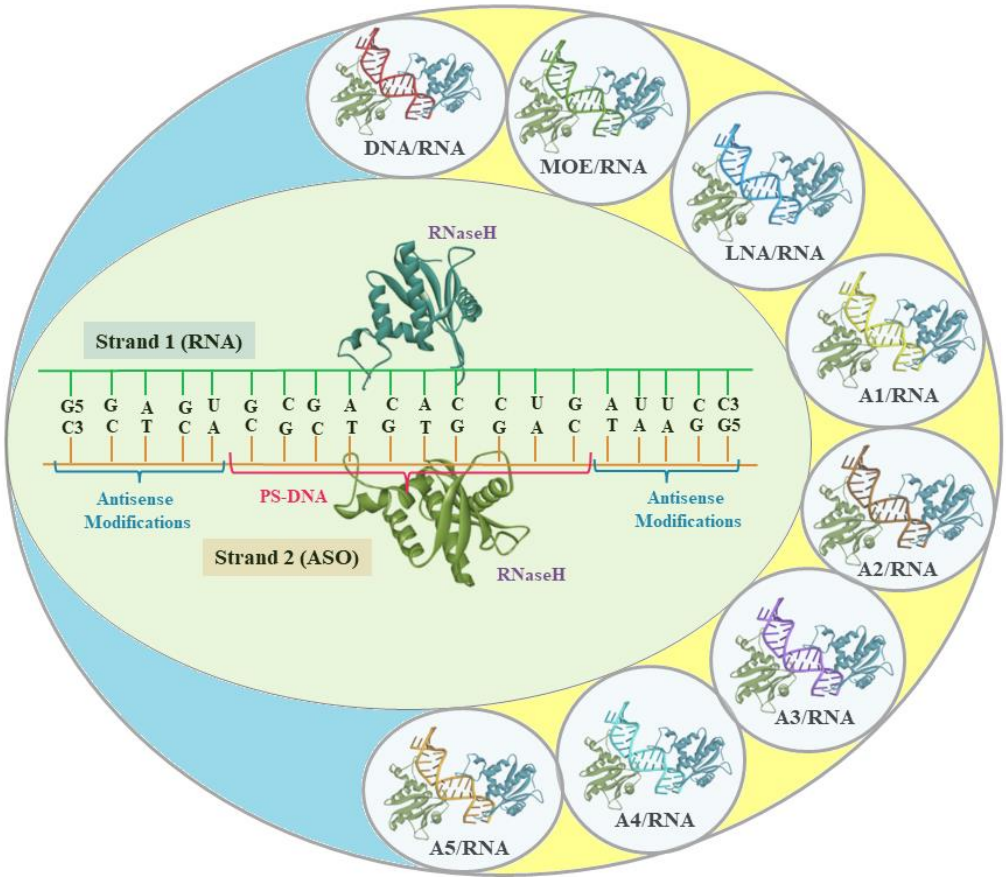

6.1. Introduction

The fundamental concept underlying antisense technology is relatively straightforward: impeding the transmission of genetic instructions from DNA to protein through complementary binding of a nucleic acid sequence to a specific mRNA using *Watson-Crick* base pair hybridization [1-2]. A majority of human disorders stem from aberrant protein synthesis or dysfunctional protein activity. Antisense oligonucleotide-based drugs (ASOs/AONs) selectively bind to their target mRNAs, possess the ability to prevent the formation of the disease-associated proteins and modulate their gene expression. By definition, ASOs/AONs can be developed to address a wide range of gene-transmitted disorders as cancer, cardiovascular diseases including numerous inflammatory and infectious ailments [3-7]. Such utilization of ASOs/AONs as a therapeutic approach represents a distinct strategy compared to the use of traditional medications [8-11]. Unlike the monoclonal antibodies and small pharmacological compounds, these synthetic ASOs/AONs collaborate with their corresponding sense mRNAs, reduce the production of disease-causing proteins, thereby achieving the intended therapeutic outcome. These antisense-driven therapeutics often exhibit greater specificity, rendering them to be more powerful and less detrimental compared to traditional medications.

Antisense oligonucleotides (ASOs/AONs) are modified nucleic acids that have been chemically altered to achieve complementarity with their target mRNAs. These mRNAs form hybrid duplexes with the ASOs through Watson-Crick base pairing. In the RNase H dependent mechanism of antisense activity, the cellular endonuclease Ribonuclease H (RNase H) catalyse the cleavage of RNA in an RNA/DNA substrate via a hydrolytic mechanism which cleave RNA backbone phosphodiester bonds to leave a 3' hydroxyl and a 5' phosphate group [12-13]. RNase H is a family of on-sequence-specific endonuclease enzymes with a shared substrate specificity for the RNA strand of DNA/RNA duplexes. When an ASO binds to an mRNA, it activates the RNase H, which selectively cleaves the RNA strand from the ASO/RNA hybrid duplexes [14-16].

The concept of using antisense oligonucleotides as therapeutic agents was first introduced by Zamecnik and Stephenson in 1978 [17]. Nevertheless, due to their inherent instability in biological environments, ASOs tend to degrade rapidly even before forming duplexes. To address this issue and ensure a robust antisense response, chemical modifications are required to enhance their stability, binding affinity, and facilitate

cellular uptake. Initially, one of the non-bridging oxygen atoms in the phosphodiester backbones of the nucleotides was replaced with a sulphur atom [18-19]. Methylphosphonates and phosphoramidates, collectively known as the first-generation ASOs, garnered considerable attention, but it was phosphorothioates (PSs) that proved to be most efficient in promoting RNase H activity [20-22]. A PS-ASO prescribed to treat cytomegalovirus-induced retinitis made history as the first antisense medication to be commercially available, under the brand name "Vitravene" (ISIS-2922), following FDA approval in 1998 [23]. However, the specificity, binding affinity, and cellular uptake of PSs occasionally fell short of expectations. As a result, second-generation ASOs were introduced to address these limitations, focusing on enhancing the pharmacokinetics of the ASOs by targeting the 2′-hydroxyl group of the furanose sugar ring. Among the most extensively studied second-generation ASOs are 2′-O-methyl (OMe) and 2′-O-methoxyethyl (MOE), known for their reduced toxicity and higher binding affinities [24-26]. To address the challenges of nuclease resistance and binding affinity, sugar-based modifications were combined with the PS backbone linkage, giving rise to chimeric ASOs [27]. This strategic fusion aimed to maximize the benefits of both approaches. Numerous FDA-approved antisense medications in the market feature these chimeric ASOs, utilizing a combination of PS-DNA and MOE modifications. The FDA has granted approval to a range of chimeric antisense medications, such as *Oblimersen, Nusinersen and Eteplirsen to* address conditions spanning cancer, spinal muscular atrophy and Duchenne muscular dystrophy [28-30]. To advance beyond the capabilities of PS and MOEs, third-generation ASOs including locked nucleic acids (LNAs), Bridged Nucleic Acids (BNAs), GuNA, morpholino oligonucleotides were developed [31-34]. LNAs are regarded as the most promising among the third-generation ASOs featuring a methylene bridge connecting the 2′-oxygen and the 4′-carbon of the furanose sugar ring, effectively securing their linkage. Comparative studies conducted by medicinal chemists considering LNA ASOs and natural oligonucleotides demonstrated enhancements in thermodynamic stability, nucleic acid recognition, water solubility, sequence specificity, biostability, and advantageous hybridization kinetics [35-37]. However, many of these constructs faced rapid degradation by nucleases and posed hepatotoxicity concerns, failing to activate the RNase H cleavage mechanism [38]. Subsequently, through structural enhancements to MOEs and LNAs, the effectiveness of these ASOs was significantly boosted, achieving a three-to-five-fold improvement (ED_{50} = 2.5 mg/kg)

without inducing hepatotoxicity [39-40]. Continuous refinement efforts in tailoring LNA structures led to the development of potent LNA analogues known as BNAs, strategically designed to overcome LNA ASO limitations. Extensive research and development have yielded promising results with 2′,4′-BNA^{NC} analogues such as 2′,4′-BNA^{NC}[NH], 2′,4′-BNA^{NC}[NMe], N-Me-aminooxy BNA, and N-MeO-amino BNA, effectively addressing the LNA ASO limitations [41-42]. In comparison, BNAs exhibit much greater nuclease resistance than PSs and LNAs. *In-vitro* and *in-vivo* studies of BNA modifications have demonstrated their superior stability at elevated temperatures, enhanced in-vitro performance, and a fivefold improvement in *in-vivo* efficacy compared to MOE ASOs. Further efforts to optimize their antisense activity continue by exploring novel modifications. Nonetheless, a comprehensive understanding of the diverse array of antisense modifications currently in use remains a critical goal for advancing the field of antisense therapeutics [43-50].

To elucidate the structural and functional significance of these ASOs a thorough investigation employing the RNase H is required. All RNases H have an active site centered on a conserved sequence motif composed of four negatively charged amino acid residues, aspartate, glutamate and a histidine residue often referred to as the DEDD motif [12-13]. By definition, these charged residues directly participate in the catalytic function, requires two metal ions for catalysis which cleave the phosphodiester bonds of RNA on either end of the cut site with a two-metal-ion catalysis mechanism involving magnesium and manganese ions under physiological conditions. Data from experiments and computer simulations suggests the enzyme uses the conserved histidine to activate a water molecule attached to one of the metal ions. The transition state, joins with the protonated phosphate and the deprotonated alkoxide leaving group to produce an intermediate. The glutamate, which has an increased pKa is used to protonate the leaving group. However, it is yet unclear how the cleft product releases itself. Henceforth, the present chapter aims to identify the important amino acid residues which might play an important role in stabilizing the duplexes at the active site of RNase H and in molecular recognition of the RNAse H in specifically identifying the RNA strand from the ASO/RNA hybrid duplexes. The goal is to evaluate the structure-activity relationship of 20-mer modified ASO/RNA hybrid gapmer-type duplexes implementing a few novel LNA-analogue antisense modifications (A1-A5), along with the standard LNA, PS-DNA and MOE antisense modifications complexed with a Human RNase H catalytic domain.

6.2. Materials and Methods

6.2.1. Force-field parameters and systems building for MD simulations

This chapter describes the structure and dynamics of modified ASO/RNA hybrid gapmer-type duplexes in complex with the Human RNase H catalytic domain. Starting structures of the duplexes were built on the crystal structure of a 20-mer RNA/DNA substrate complexed with Human RNase H1 catalytic domain (PDB ID: 2QKB as reported by *Nowotny et al.*) [13]. The built in duplexes include wild type DNA/DNA, RNA/DNA, RNA/RNA duplexes and modified ASO/RNA hybrid gapmer-type duplexes containing five novel LNA-based antisense modifications A1, A2, A3, A4, A5 along with the standard LNA and MOE antisense modifications. In modifications A1-A5, the 2′-carbon and 4′-carbon of the sugar moiety are linked by five different conformationally constrained functional groups implemented considering the PS backbone linkage where one of the non-bridging oxygen atoms from the sugar-phosphate backbone was replaced by Sulphur. The modifications are LNA based. In all the modifications, the 2′-oxygen and 4′-carbon of the ribose sugar ring are linked to each other by five different conformationally constrained functional groups, designed by infusing different oxy or nitro groups into the parent LNA structure. In accordance with the five nucleobases, force-field parameters for the antisense alterations A1-A5 were developed and reported in literature [50]. The AMBER software programs all-atom MD simulation framework was used for building of the duplexes and running the MD simulations [51]. Gaussian09 software was used to derive partial atomic charges at the M06-2X/-311G** level of theory and RESP fitting was completed using the antechamber module of AMBER [52-53]. Five residues from ASO strand's 5′ and 3′ end was specifically modified integrating them into gapmer-type duplexes. The systems were explicitly solvated with TIP3P water boxes after the charge was neutralized by the addition of Na^+/Cl^- as counter ions [54]. Using the leap module, the complete duplex building process was carried out implementing the standard force field parameters "DNA.OL15" for DNA, "RNA.OL3" for RNA, and using developed force-field parameters for the A1-A5 antisense alterations [50,55-56].

6.2.2. Simulation Protocol and Trajectories Analyses

The built in systems were energy minimized to create correct initial structures wherein initial positional restrictions of 100 kcal/mol were used to keep the solute atoms stable,

which was then followed by a gradual reduction and eventual removal of all restrictions. Energies were minimized using the steepest descent method for 5000 steps. The systems were then heated gradually from 0 K to 300 K in NVT canonical ensemble with 100 kcal/mol limitations on each solute atom. Following heating, the systems proceeded through equilibration with initial restrictions of 100 kcal/mol and gradually relaxing the constraints on every solute atom in NPT conditions. The systems were then allowed to simulate under production run conditions for 1 μs simulation time and the trajectories were used for analysis. Particle Mesh Ewald approach was used to simulate the system under periodic boundary conditions while taking the long-range electrostatics into consideration [57]. The SHAKE method was used to perform MD integration with a 2.0 fs time step on all bonds containing hydrogen atoms [58]. Langevin temperature equilibration scheme was used to maintain the system temperature. The cut-off distance for non-bonding encounters has been set at 10. NPT conditions were maintained throughout the production simulation run and the pair-list was updated at every 5000 steps. To account for the statistical variance in the computations, replica sets of MD simulations accounting to two data sets Set-I & Set-II were performed, each trajectory corresponding to 1 μs simulation time. The RMSD, RMSF, sugar pucker, N-glycosidic dihedral angles, inter-strand and intra-strand phosphate distances, H-bonds, Solvent Accessible Surface Area (SASA) all were computed using the CPPTRAJ module of Amber Tools [59]. Base-pairing, Base-stacking and Helix-turning all were observed using the NASTRUCT module of AMBER. The free energies of all the duplexes were calculated using the MMGBSA module of AMBER [60].

6.3. Results and Discussion

This chapter discusses the dynamic properties and energetics of the 20-mer ASO/RNA hybrid gapmer-type duplexes in complex with RNase H implementing the designed antisense modifications (A1-A5) along with the standard antisense modifications PS-DNA, MOE and LNA as the control systems [50]. In modifications A1-A5, the 2′-carbon and 4′-carbon of the sugar moiety are linked by five different conformationally constrained functional groups. All the modifications were implemented considering the PS backbone linkage where one of the non-bridging oxygen atoms from the sugar-phosphate backbone was replaced by Sulphur. The modified residues were inserted in five residues from ASO strand's 5′ and 3′ end keeping the middle ten residues PS-DNA modified resulting into gapmer-type duplexes, depicted in Scheme 6.1.

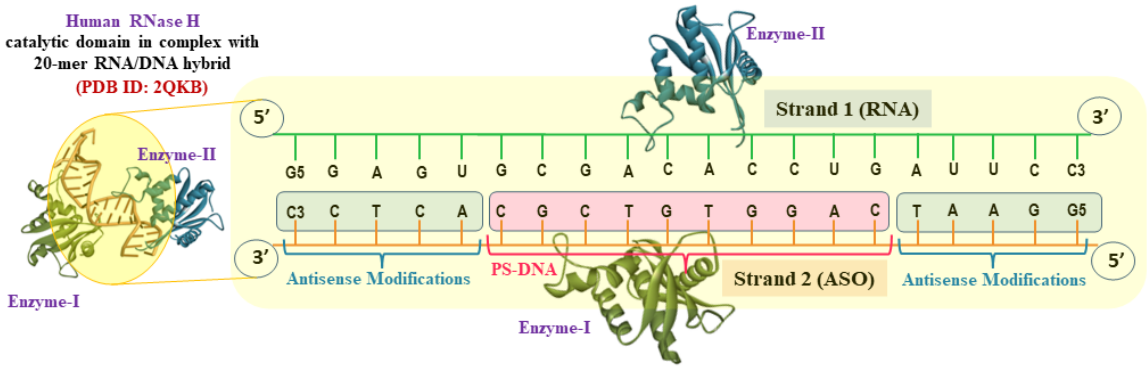

Scheme 6.1: A Schematic representation of the modified ASO/RNA hybrid gapmer-type duplexes complexed with dimeric RNase H [Enzyme I & Enzyme-II] catalytic domain.

6.3.1. Stability of the modified ASO/RNA hybrid gapmer-type duplexes

Simulations were conducted for eight modified ASO/RNA hybrid gapmer-type duplexes complexed with the RNase H (a) PS-DNA/RNA-RNaseH (b) PS-MOE/RNA-RNaseH (c) PS-LNA/RNA-RNaseH (d) PS-A1/RNA-RNaseH (e) PS-A2/RNA-RNaseH (f) PS-A3/RNA-RNaseH (g) PS-A4/RNA-RNaseH and (h) PS-A5/RNA-RNaseH. To understand how the ASO/RNA duplexes structural characteristics changed over the course of the simulation, structures of the duplexes have been pictured at 500th ns and 1000th ns from the 1 μs simulation trajectory, plotted in Figure 6.1, for both of the simulation sets (Set-I & Set-II). An unligated RNase H was also considered for the simulations for comparison. From Figure 6.1 it was observed of the ASO/RNA duplexes to be stable at the catalytic domain of RNase H maintaining stable *Watson-Crick* base-pairing, base-stacking pattern and helix-turning throughout the simulation time.

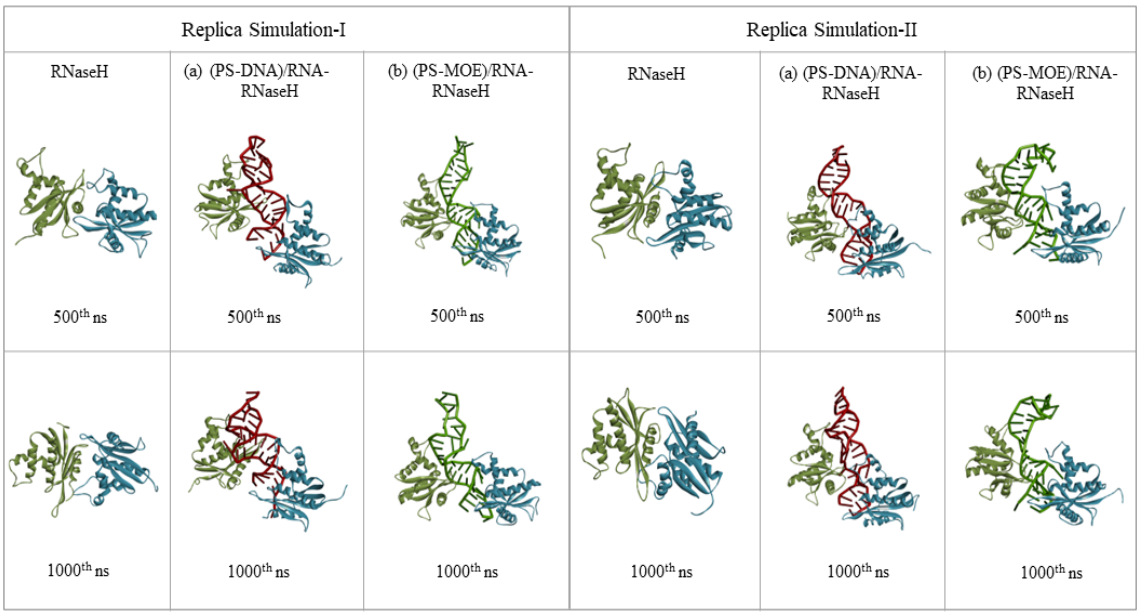

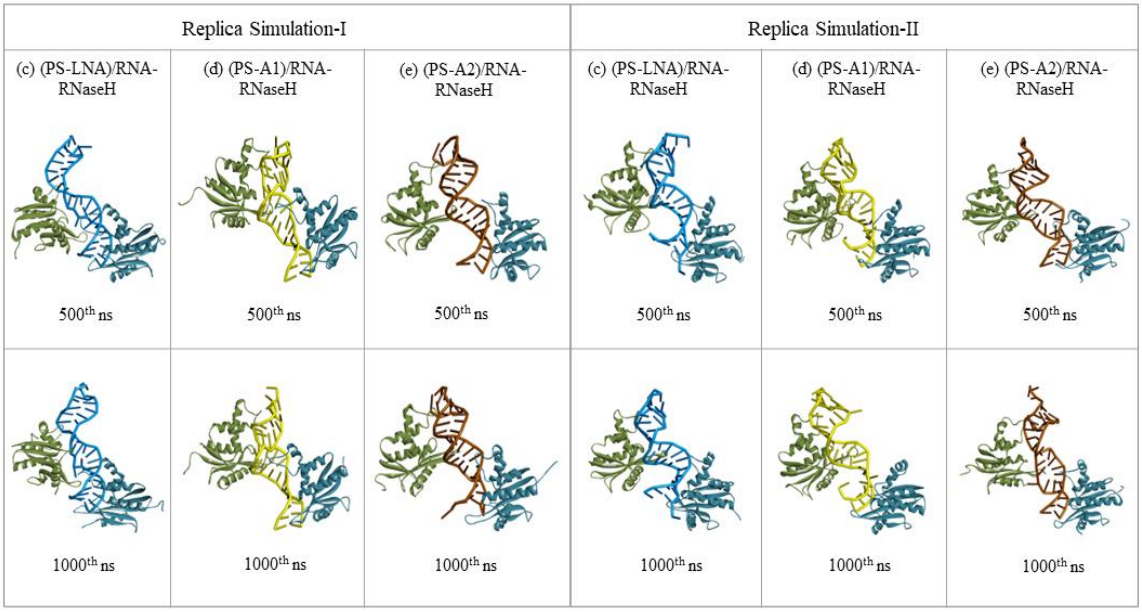

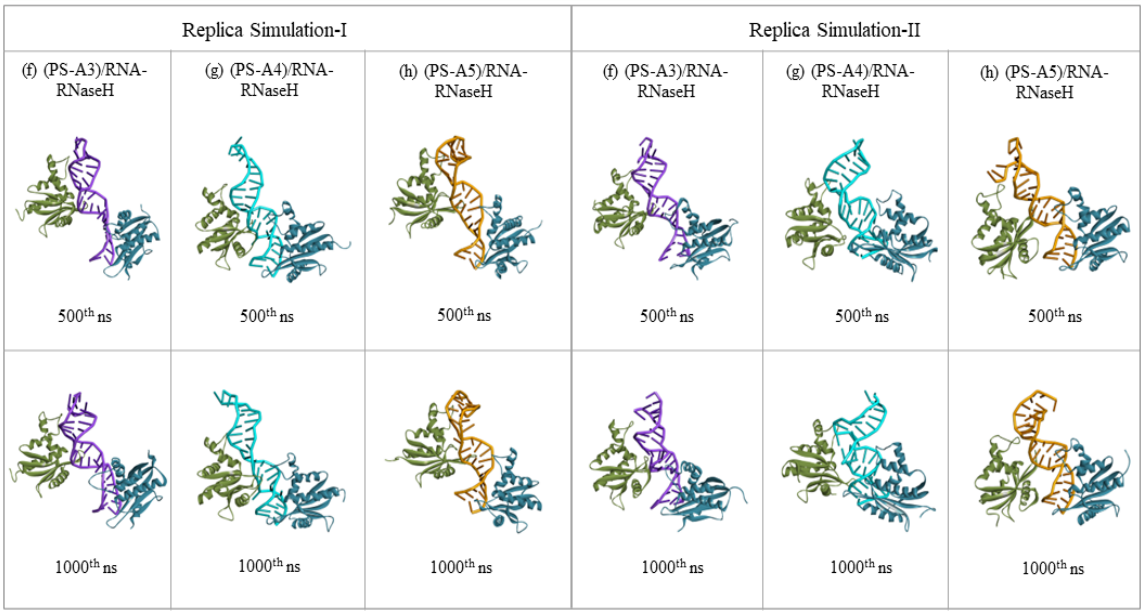

Figure 6.1: Structures of the ASO/RNA duplexes (a) PS-DNA/RNA-RNaseH (b) PS-MOE/RNA-RNaseH (c) PS-LNA/RNA-RNaseH (d) PS-A1/RNA-RNaseH (e) PS-A2/RNA-RNaseH (f) PS-A3/RNA-RNaseH (g) PS-A4/RNA-RNaseH and (h) PS-A5/RNA-RNaseH complexed with dimeric RNaseH at 500th ns and end structures at 1000th ns obtained from the 1µs simulation trajectory, for both the sets of simulation [Set-I & Set-II].

The structures acquired from the complete simulation trajectory were compared with their respective initial structures reviewing the RMSD plots encompassing the whole duplex presented in Figure 6.2 and RMSD plots of the RNaseH alone are plotted in Figure 6.3. Each of the duplexes appeared to be fluctuating potentially within and around a range of 2 to 6 Å RMSD values with an exception for the PS-MOE/RNA duplex. Calculated average RMSD values of the systems (a)-(h) exhibited an average RMSD of 5.16, 7.04, 5.55, 5.84, 3.88, 6.29, 4.66 and 4.90 Å and 4.84, 8.03, 4.23, 4.36, 5.22, 5.58, 5.95 and 5.15 Å for Set-I and Set-II, respectively. RMSD of PS-MOE is higher for both the sets of simulation whilst rest of the duplexes are exhibiting relatively similar RMSDs compared to the PS-DNA and PS-LNA/RNA control systems. The ASO/RNA duplexes overall RMSD data over time indicated that duplex stability is well preserved in each case for the entire duration of the simulation for both the sets of simulation.

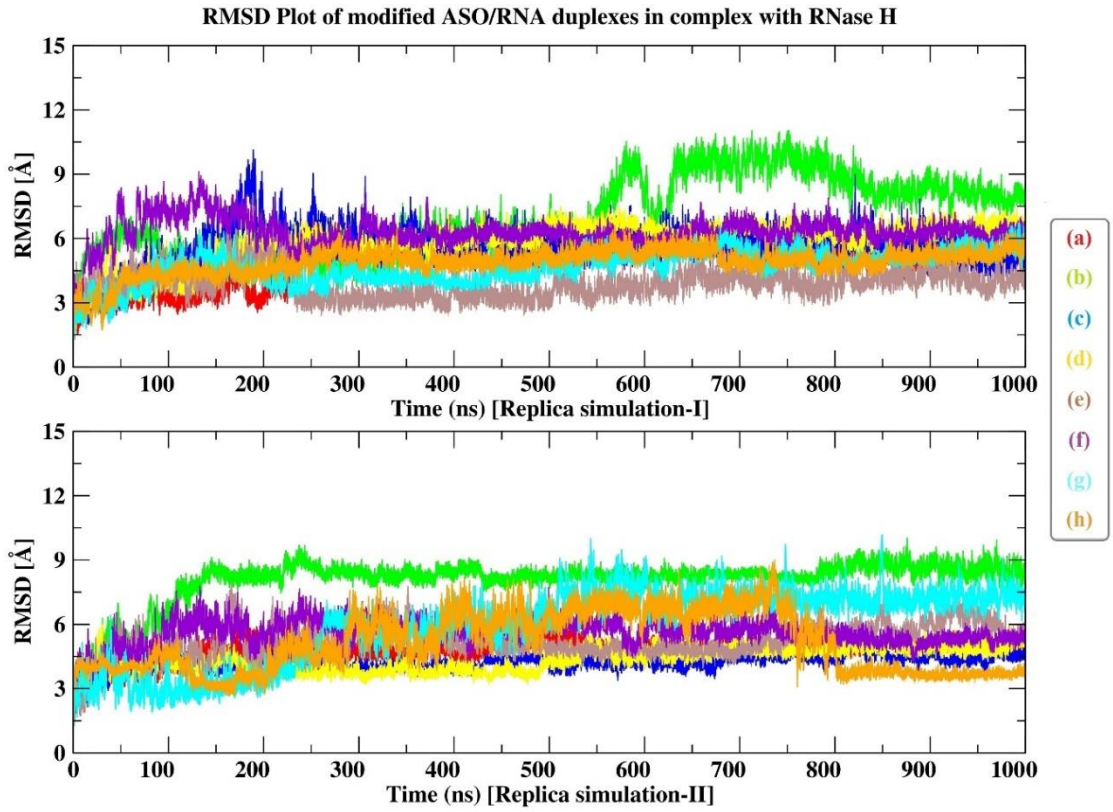

Figure 6.2: RMSD plots of the ASO/RNA duplexes (a) PS-DNA/RNA-RNaseH (b) PS-MOE/RNA-RNaseH (c) PS-LNA/RNA-RNaseH (d) PS-A1/RNA-RNaseH (e) PS-A2/RNA-RNaseH (f) PS-A3/RNA-RNaseH (g) PS-A4/RNA-RNaseH and (h) PS-A5/RNA-RNaseH of simulation trajectories from two data sets [I & II] each simulated for 1 μs simulation time.

In Figure 6.2, the average RMSD values for (b) PS-MOE/RNA-RNaseH is higher compared to rest of the complexes for the both sets of simulation. 2'-O-methoxyethyl (MOE) is a chemical modification involving the addition of a methoxyethyl group at the 2'-position of the ribose sugar in RNA or DNA molecules.

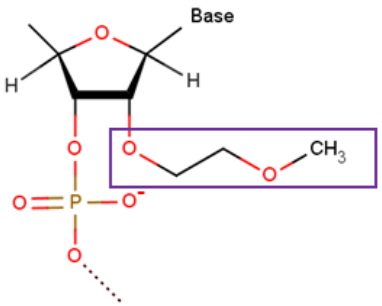

2'-O-methoxy-ethyl RNA
(MOE)

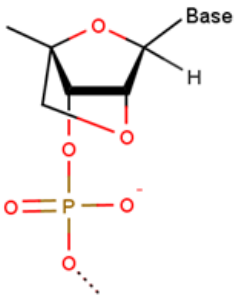

Locked Nucleic Acid
(LNA)

The higher RMSDs associated with MOE modifications compared to the rest of the ASO/RNA duplexes can be attributed to bulkiness of the MOE group, inducing changes in backbone flexibility, steric hindrance, and interactions with the surrounding environment. The addition of the methoxyethyl group at the 2'-position of the ribose sugar introduces bulkiness to the nucleic acid molecule. This bulkiness leads to increased steric hindrance and alterations in the conformational dynamics of the molecule. MOE modifications also introduce conformational heterogeneity, resulting in a broader range of structural states as the molecule explores a larger conformational space. This increased conformational heterogeneity results in higher RMSDs sampled during MD simulations. Rest of the modifications are LNA, BNA modified RNA nucleotides which have a bridge artificially added at the 2' and 4' positions of the ribose to produce restricted RNA molecules. LNA, BNAs are known for their enhanced stability due to the presence of a methylene bridge that locks the ribose ring in the C3'-endo sugar conformation. Additionally, LNAs are known to exhibit stronger hybridization with complementary nucleic acid sequences compared to unmodified DNA or RNA. This increased stability can lead to fewer conformational changes and the enhanced binding can lead to more stable secondary structures, lowering their RMSD fluctuations over time. Thus, the MOE modified duplexes were exhibiting higher deviations compared to the rest of the systems. The presence of such bulky group as MOEs may also influence the interactions between the modified nucleic acid molecule and its surrounding environment, such as solvent molecules or binding partners.

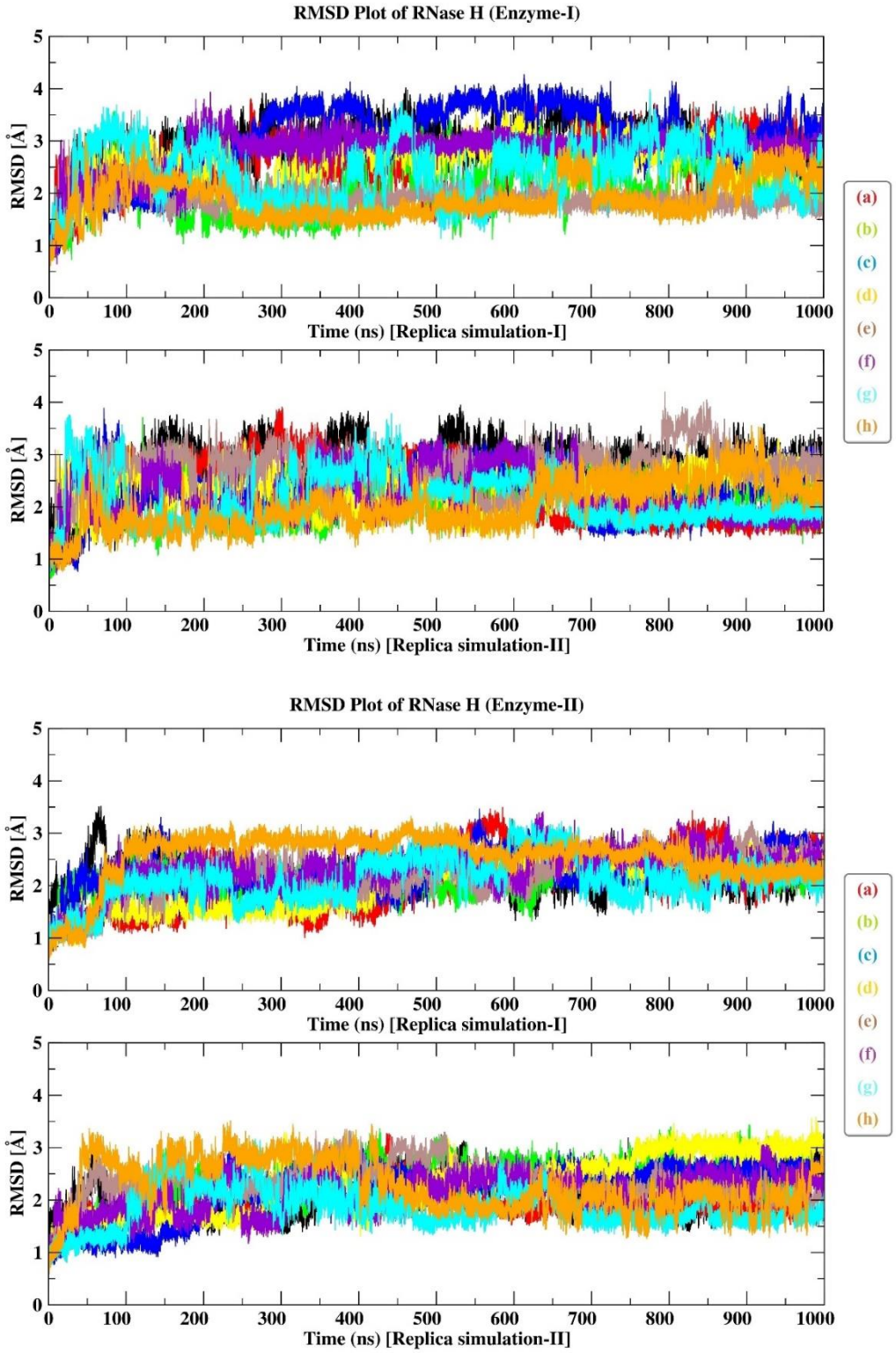

Figure 6.3: RMSD plots of the RNase H alone from the (a) PS-DNA/RNA-RNaseH (b) PS-MOE/RNA-RNaseH (c) PS-LNA/RNA-RNaseH (d) PS-A1/RNA-RNaseH (e) PS-A2/RNA-RNaseH (f) PS-A3/RNA-RNaseH (g) PS-A4/RNA-RNaseH and (h) PS-A5/RNA-RNaseH complexes of simulation trajectories from two data sets [Set-I & Set-II] each simulated for 1 μs simulation time.

6.3.2. MM-GBSA of the modified ASO/RNA hybrid gapmer-type duplexes

Using MM-GBSA, one can theoretically estimate the binding affinities between the ASO and the target RNA sequence, which is crucial for designing ASOs with optimal binding properties. While it's commonly applied to study protein-ligand interactions, it can also be adapted for protein-protein, protein-RNA or ASO/RNA duplexes. However, it's important to note that MM-GBSA predictions are approximations and may not always accurately reflect experimental binding affinities. The MM-GBSA binding free energy values for each of the ASO/RNA duplexes in complex with RNase H were calculated taking into account the complete simulation trajectory presented in Table 6.1.

Table 6.1: MM-GBSA of the ASO/RNA duplexes (a) PS-DNA/RNA-RNaseH (b) PS-MOE/RNA-RNaseH (c) PS-LNA/RNA-RNaseH (d) PS-A1/RNA-RNaseH (e) PS-A2/RNA-RNaseH (f) PS-A3/RNA-RNaseH (g) PS-A4/RNA-RNaseH and (h) PS-A5/RNA-RNaseH of simulation trajectories from data sets [Set-I & Set-II] each simulated for 1 μs simulation time.

Name Code	Replica Simulation-I			
	$G_{(ASO/RNA)-RNaseH}$	G_{RNaseH}	$G_{ASO/RNA}$	ΔG
(a) PS-DNA/RNA-RNaseH	-15604.94	-7568.13	-7824.22	-212.59
(b) PS-MOE/RNA-RNaseH	-14862.60	-7592.78	-7037.51	-232.31
(c) PS-LNA/RNA-RNaseH	-14944.52	-7593.77	-7215.49	-135.27
(d) PS-A1/RNA-RNaseH	-15198.79	-7592.54	-7420.24	-186.01
(e) PS-A2/RNA-RNaseH	-15214.74	-7599.88	-7389.26	-225.59
(f) PS-A3/RNA-RNaseH	-15024.58	-7585.01	-7236.79	-202.78
(g) PS-A4/RNA-RNaseH	-15576.39	-7605.26	-7767.59	-203.54
(h) PS-A5/RNA-RNaseH	-15304.55	-7625.42	-7473.23	-205.90
Name Code	**Replica Simulation-II**			
	$G_{(ASO/RNA)-RNaseH}$	G_{RNaseH}	$G_{ASO/RNA}$	ΔG
(a) PS-DNA/RNA-RNaseH	-15537.88	-7579.03	-7835.46	-123.39
(b) PS-MOE/RNA-RNaseH	-14864.54	-7604.85	-7024.81	-234.88
(c) PS-LNA/RNA-RNaseH	-14988.52	-7591.53	-7167.87	-229.11
(d) PS-A1/RNA-RNaseH	-15165.51	-7572.02	-7368.55	-224.95
(e) PS-A2/RNA-RNaseH	-15172.03	-7599.10	-7383.10	-189.83
(f) PS-A3/RNA-RNaseH	-15020.71	-7603.49	-7239.14	-178.08
(g) PS-A4/RNA-RNaseH	-15560.77	-7599.93	-7780.14	-180.70
(h) PS-A5/RNA-RNaseH	-15232.37	-7598.78	-7445.29	-188.30

MM-GBSA binding free energy values of all the ASO/RNA duplexes for the entire simulation trajectory were calculated considering the RNase H as the target protein receptor, the modified ASO/RNA duplexes as the binding ligand and the ASO/RNA duplexes in complex with the RNase H as the receptor-ligand complex. In case of modified ASO/RNA duplexes, RNase H is activated by the ASO/RNA duplexes which then specifically cleaves the RNA strand from the ASO/RNA duplexes in a targeted manner. In Table 6.1, free energy (G) of RNase H has nearly identical energy values and free energy of the ASO/RNA duplexes varied depending on the type of antisense alterations. Free energy of PS-DNA/RNA is highest negative and PS-MOE/RNA is lowest negative. PS-DNA being an immediate analogue of natural DNA is exhibiting the highest stability as natural DNA compared to the rest of the modifications for both Set-I & Set-II simulation trajectories. Next to PS-DNA, A4 modification is exhibiting higher stability for both Set-I & Set-II simulation trajectories. A1, A2, A5 have almost similar free energies and A3 has the lowest free energy among the proposed modifications, suggesting A3 modifications to be less stable comparatively. These modifications are LNA modified RNA nucleotides known for their enhanced stability due to the presence of a methylene bridge that locks the ribose ring in the C3'-endo sugar conformation leading to fewer conformational changes which can lead to more stable secondary structures, lowering their RMSD fluctuations over time. Additionally functionalising them have stabilized the modifications over PS-LNA modifications. PS-LNA is exhibiting lower stability compared to the proposed modifications and almost nearing PS-MOE modifications for both Set-I & Set-II simulation trajectories. As already discussed, higher RMSDs associated with PS-MOE modifications compared to the rest of the ASO/RNA duplexes were observed due to bulkiness of the MOE group. Accordingly, free energy of PS-MOE modified ASO strand is indicative of higher deviation or movement of the MOE modified ASO strand. However, the free energy of binding (ΔG) is the highest for the PS-MOE/RNA-RNaseH system, for both Set-I & Set-II simulation trajectories.

Overall, MM-GBSA binding energies estimated for the entire simulation trajectory predicted that modifications PS-DNA, PS-A2, PS-A3, PS-A4 and PS-A5 from Set-I and PS-LNA and PS-A1 from Set-II have comparable ΔG values with the PS-MOE modifications. Thus, depending on these results one may infer that the suggested modifications are as stable as MOEs.

6.3.3. Oligomer Duplex Dynamic Structure: Inter-Strand and Intra-Strand PP distances of the modified ASO/RNA hybrid gapmer-type duplexes

Structural framework of the duplexes described by the molecular double helix of the nucleic acids elucidate the overall width of the duplex as well as the major and minor groove width of the helices. To observe the structural framework of the modified ASO/RNA duplexes, average inter-PP and intra-PP distances for both the strands for the entire simulation trajectory are plotted in Figure 6.4 and Figure 6.5 respectively. Inter-strand PP distances of the duplexes for both the sets of simulation were varying in case of the ASO/RNA duplexes compared to wild type duplexes. Longer intra-strand PP distances (~7 Å) are used to explain the *C2′-endo* sugar puckering observed in *B-type* duplexes, while shorter intra-PP distances (~5.9 Å) are used to describe the *C3′-endo* sugar puckering observed in *A-type* duplexes [61-62]. The residues are highly fluctuating however no residue exhibited intra-PP distance > 7 Å, thus the residues were maintaining *C3′-endo* conformation throughout the simulation.

The orientation of the sugar-phosphate backbone in relation to the sugar or the nucleobases and the nucleotide distribution puckering are closely related to the oligomer duplex structure. The *A-form* and *B-form* conformations in a duplex, respectively, are represented by the sugar puckers in nucleic acids, which are either in the *C3′-endo* conformation (pucker phase values: 0°–40°) or the *C2′-endo* conformation (pucker phase values: 120°–180°) [63-64]. In an effort to establish an overall *B-form* geometry, DNA type resides drive a larger population of sugar puckers into the *C2′-endo* conformation, whereas RNA type resides drives a larger population of sugar puckers into the *C3′-endo* conformation. The connections between the nucleotides sugar-puckering and *N-glycosidic* dihedral angles are a clear reflection of the variations in non-bonded conflicts brought on by the *C2′-endo* versus *C3′-endo* conformations. The N-glycosidic dihedral angle chi (χ) measures the impact of variations on the distance between atoms directly attached to the C1′ carbon that forms the glycosidic bond with RNA. The sugar and nucleobase are two separate objects having an internal degree of freedom, as evidenced by the N-glycosidic bond and its chi (χ) torsion angle. Although chi (χ) can adopt a wide range of values, structural constraints limit the values that chi (χ) can adopt given explicitly stated preferences. Syn glycosidic angles are unusual in nucleotides with C3′-endo sugar puckers because of the steric conflict between the nucleobase and the H3′ atom, which is directed towards the base in this particular pucker mode.

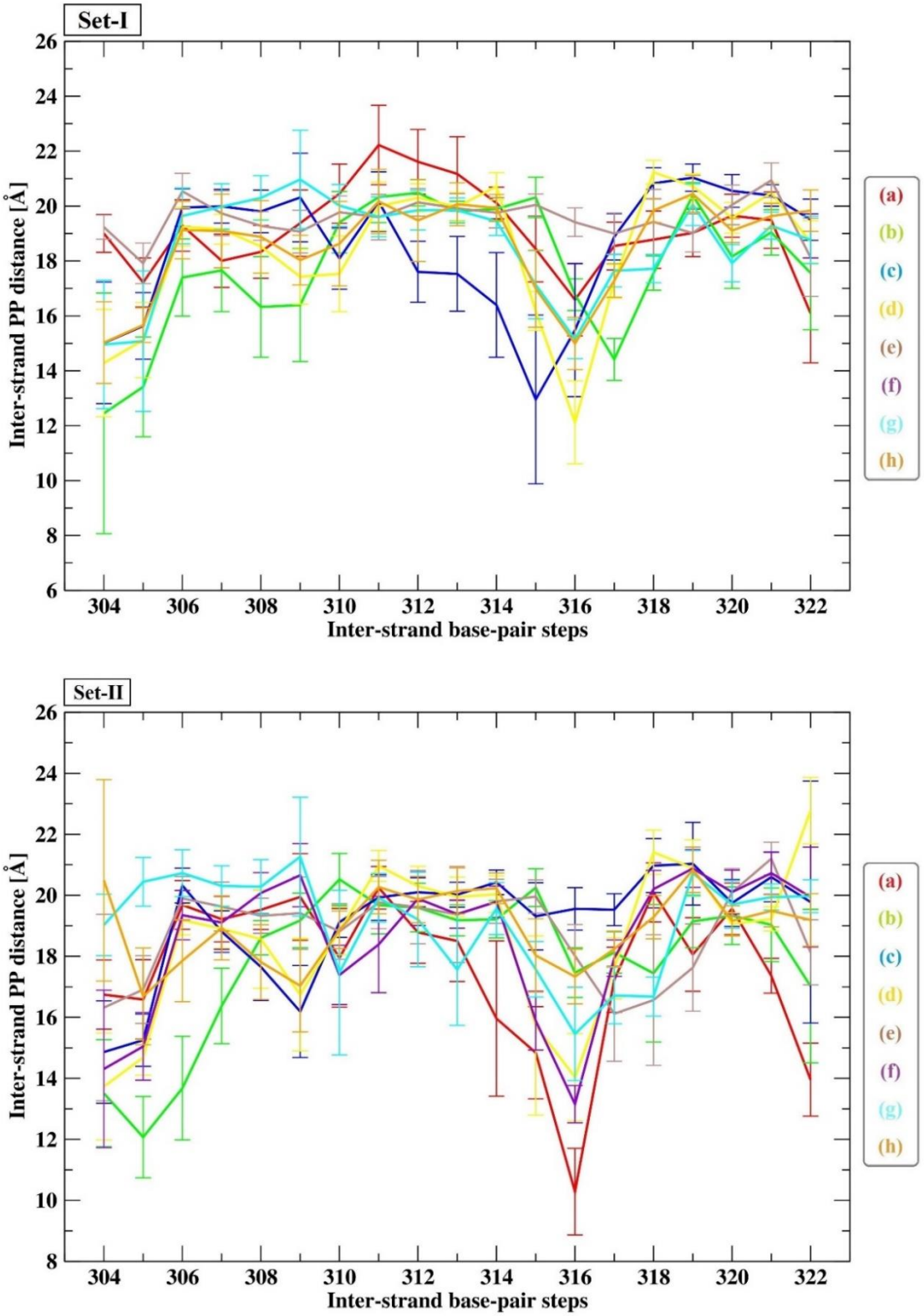

Figure 6.4: Inter-strand PP distances of the RNase H alone from the (a) PS-DNA/RNA-RNaseH (b) PS-MOE/RNA-RNaseH (c) PS-LNA/RNA-RNaseH (d) PS-A1/RNA-RNaseH (e) PS-A2/RNA-RNaseH (f) PS-A3/RNA-RNaseH (g) PS-A4/RNA-RNaseH and (h) PS-A5/RNA-RNaseH complexes of simulation trajectories from two data sets [Set-I & Set-II] each simulated for 1 μs simulation time.

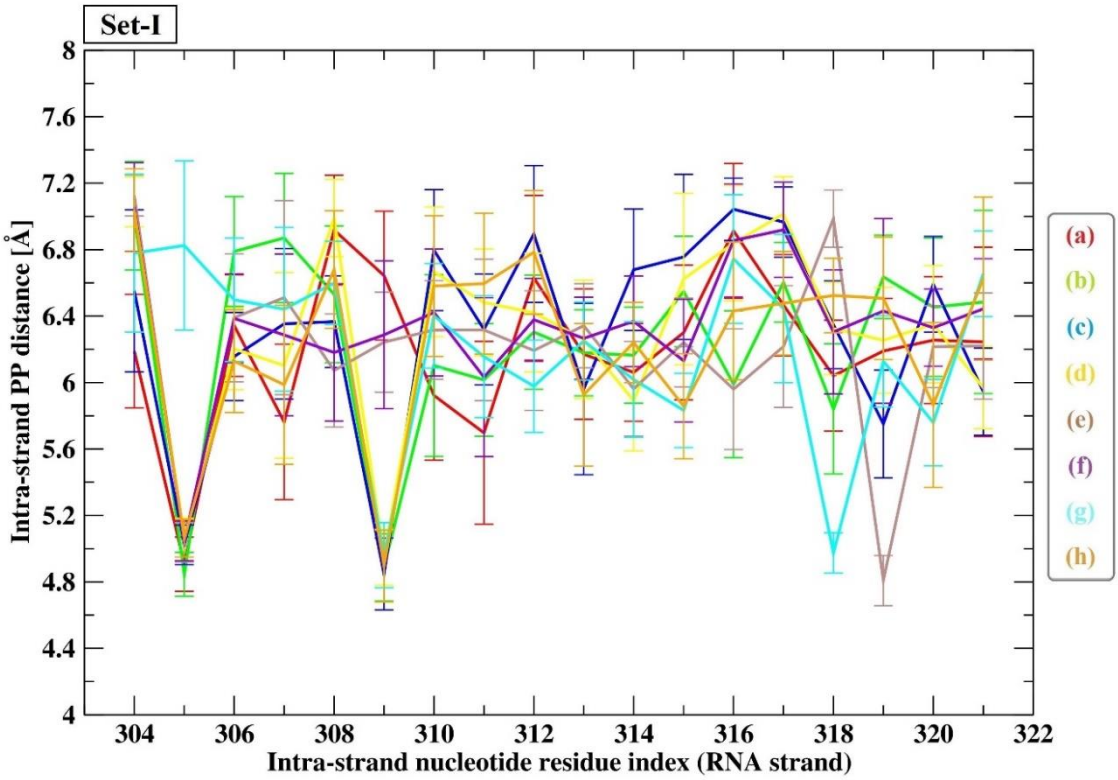
Set-I
Intra-strand PP distance [Å]
Intra-strand nucleotide residue index (RNA strand)
(a)
(b)
(c)
(d)
(e)
(f)
(g)
(h)

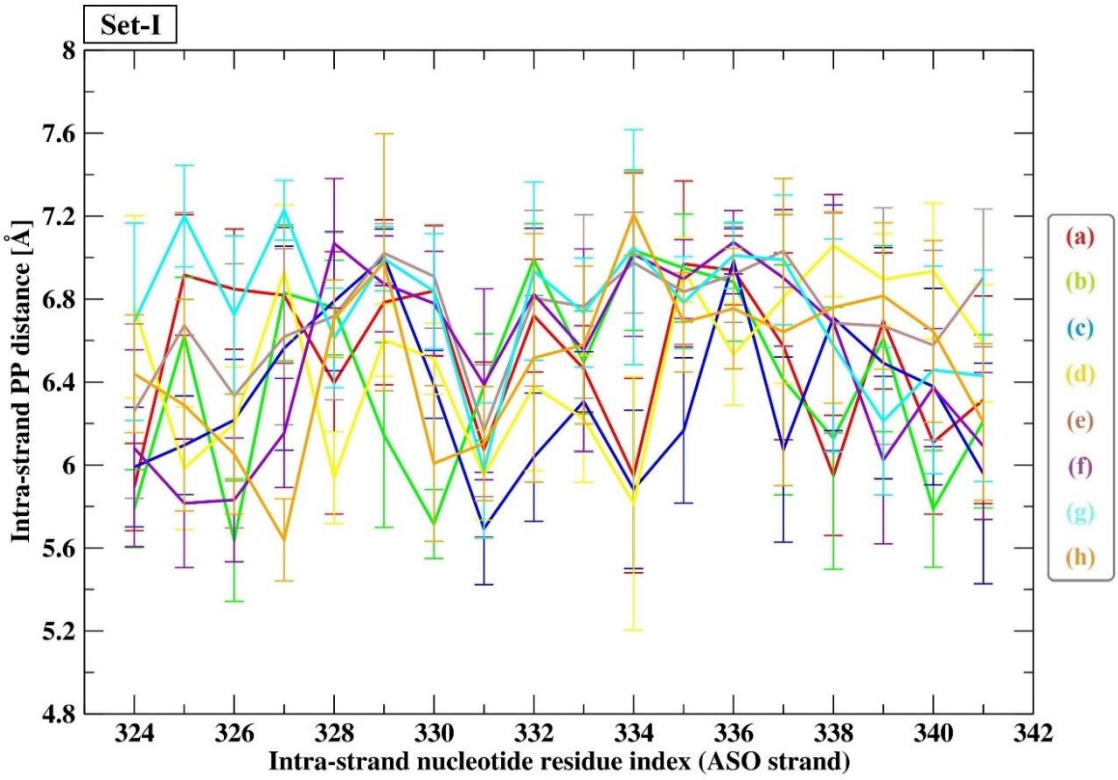
Set-I
Intra-strand PP distance [Å]
Intra-strand nucleotide residue index (ASO strand)
(a)
(b)
(c)
(d)
(e)
(f)
(g)
(h)

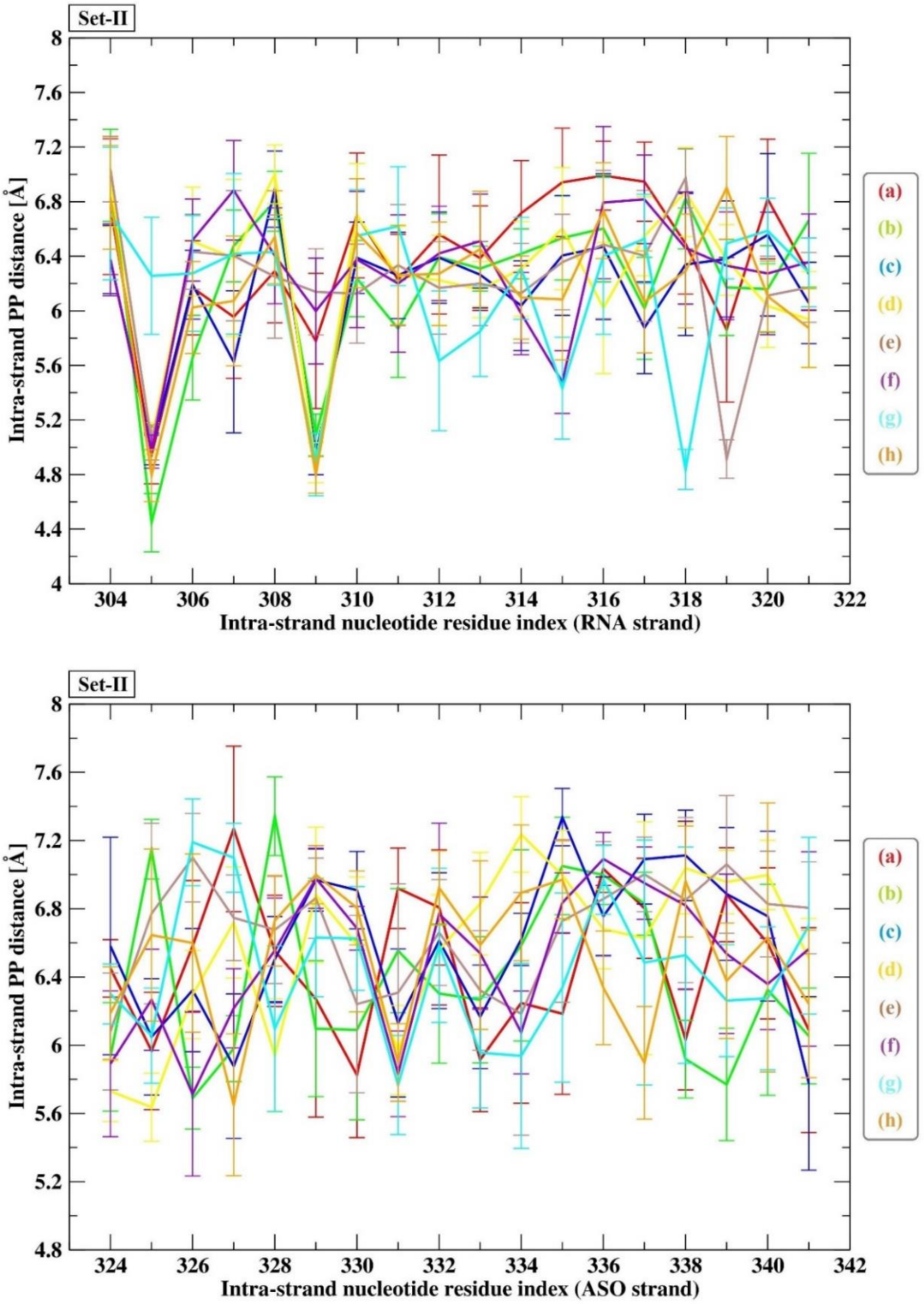

Figure 6.5: Intra-strand PP distance of the ASO/RNA duplexes (a) PS-DNA/RNA-RNaseH (b) PS-MOE/RNA-RNaseH (c) PS-LNA/RNA-RNaseH (d) PS-A1/RNA-RNaseH (e) PS-A2/RNA-RNaseH (f) PS-A3/RNA-RNaseH (g) PS-A4/RNA-RNaseH and (h) PS-A5/RNA-RNaseH of simulation trajectories from two data sets [Set-I & Set-II] each simulated for 1 μs simulation time.

6.3.4. Torsion Angle Dynamics: Sugar-pucker and N-glycosidic torsion distribution of the modified ASO/RNA hybrid gapmer-type duplexes

To estimate the extent of conformational integration of the ASO/RNA duplexes, sugar pucker distribution of the nucleotide residues throughout the duplex are presented in Figure 6.6. In Figure 6.6, terminal residues from either end of the ASO strand of the duplex systems (a) and (b) are PS-DNA and PS-MOE modifications exhibiting *C2'-endo* conformation. Duplexes (c)-(h) are LNA and LNA-based contained antisense modifications expected to exhibit *C3'-endo* conformation. Accordingly, terminal residues from either end of the ASO strand of the duplex systems (c)-(h) are exhibiting strictly *C3'-endo* conformation throughout the simulation. The PS-DNA modified non-terminal residues from the ASO strands (a)-(h) are exhibiting *C2'-endo* conformation, as expected. On the other hand, the RNA strand residues from the ASO/RNA duplexes for all the duplex systems is expected to exhibit *C3'-endo* conformation for all the residues i.e., for both the non-terminal as well as the terminal residues from the complete strand. Compared to the RNA strand of the wild type duplexes, the RNA strand residues of the modified ASO/RNA duplexes although majority were exhibiting *C3'-endo* conformation, few are seen to fluctuate from the ideal *C3'-endo* conformation exhibiting a in between *C3'-endo* and the *C2'-endo* conformations. Overall, the RNA strand residues are influenced by their complementary ASO strand residues, for both the terminal and the non-terminal residues.

To examine the rigidity of the nucleotide residues across the duplex the N-glycosidic torsion distribution of the monomer nucleotides from both strands of the ASO/RNA duplexes is presented in Figure 6.7. As already discussed, two primary low-energy conformations for the *A-form* and *B-form* duplexes, where ranges of +90° to +180° and -90° to -180° belong to the *anti*-conformation while values in the range of -90° to +90° relate to the *syn*-conformation. Figure 6.7 shows that the monomer nucleotides from the ASO strand have chi (χ) values ranging from -120° to -180° and the RNA strand residues have values ranging from -60° to -180°, both of which indicate that the residues are in an *anti*-conformation. The duplexes attempted to maintain their relative sugar-base orientations to be in anti-conformation throughout the duration of the simulation, despite residues from the ASO strands containing the antisense modifications being observed influencing the N-glycosidic torsion distribution on their complementary RNA strands.

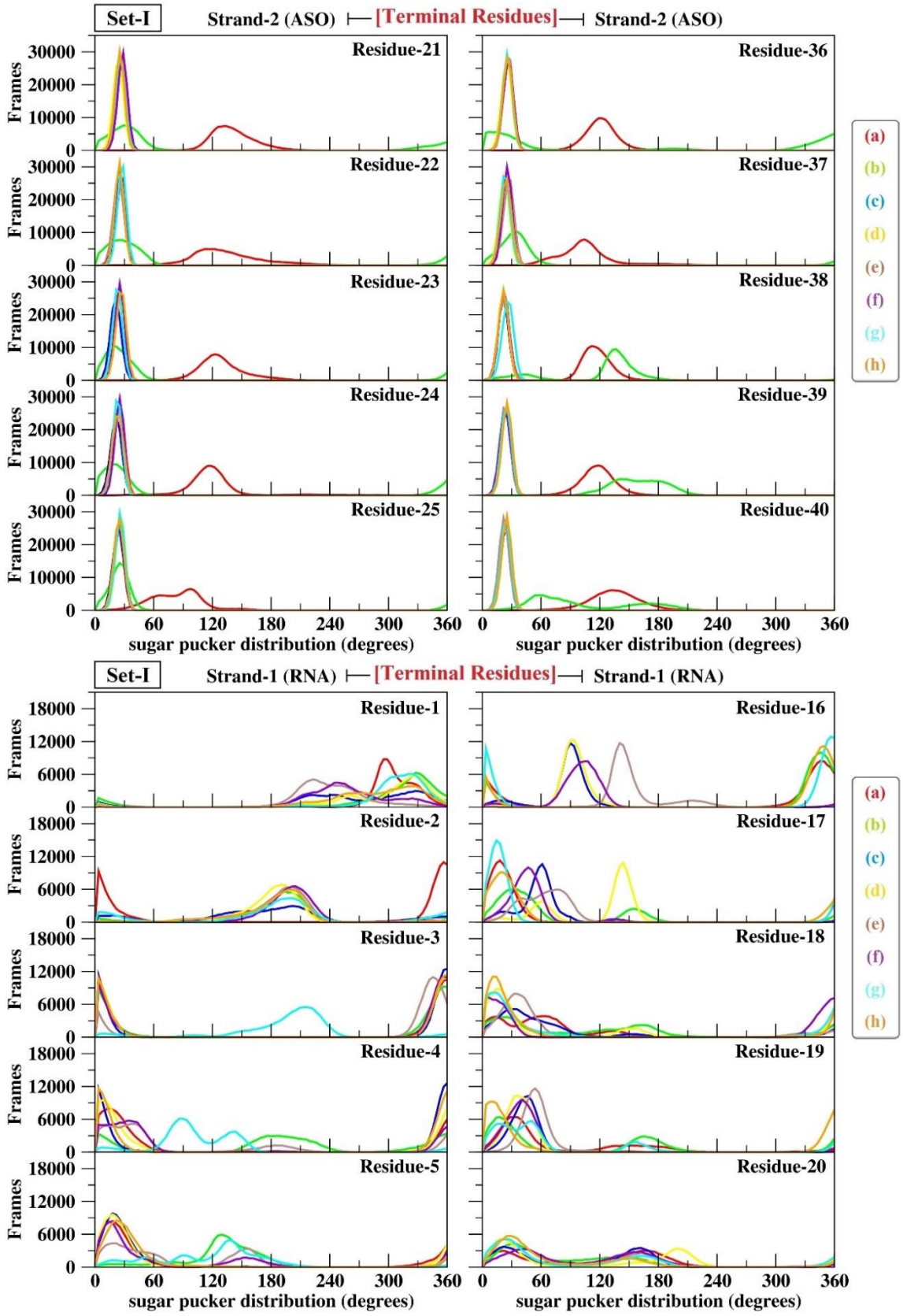
Set-I
Strand-2 (ASO) ⊢ [Terminal Residues] ⊣ Strand-2 (ASO)
Residue-21
Residue-22
Residue-23
Residue-24
Residue-25
Residue-36
Residue-37
Residue-38
Residue-39
Residue-40
Frames
30000
20000
10000
0
0 60 120 180 240 300 360
sugar pucker distribution (degrees)
(a)
(b)
(c)
(d)
(e)
(f)
(g)
(h)
Set-I
Strand-1 (RNA) ⊢ [Terminal Residues] ⊣ Strand-1 (RNA)
Residue-1
Residue-2
Residue-3
Residue-4
Residue-5
Residue-16
Residue-17
Residue-18
Residue-19
Residue-20
Frames
18000
12000
6000
0
0 60 120 180 240 300 360
sugar pucker distribution (degrees)
(a)
(b)
(c)
(d)
(e)
(f)
(g)
(h)

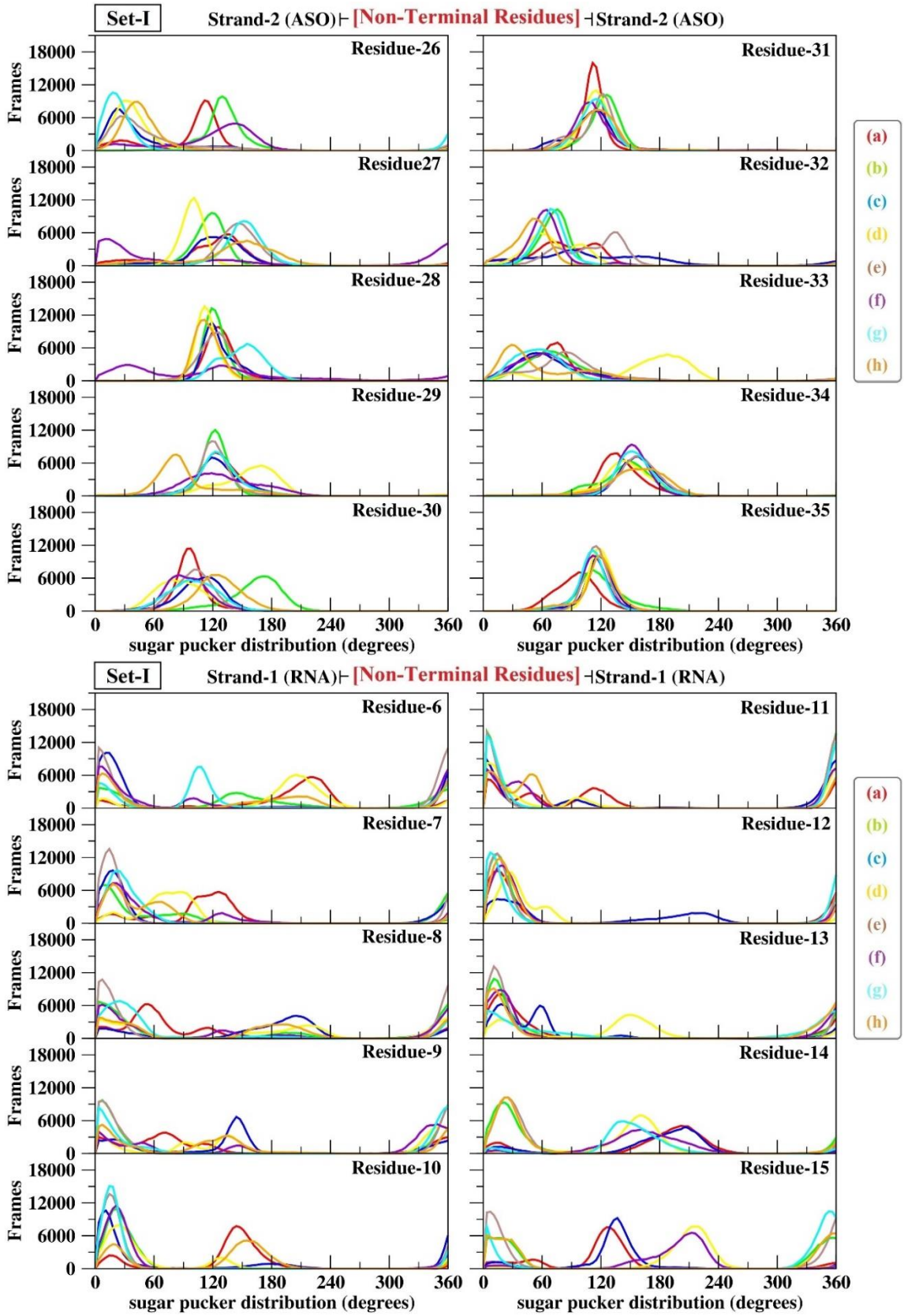
Set-I
Strand-2 (ASO)⊢ [Non-Terminal Residues] ⊣Strand-2 (ASO)
Residue-26
Residue-31
Residue27
Residue-32
Residue-28
Residue-33
Residue-29
Residue-34
Residue-30
Residue-35
Frames
18000
12000
6000
0
0 60 120 180 240 300 360
sugar pucker distribution (degrees)
(a)
(b)
(c)
(d)
(e)
(f)
(g)
(h)
Set-I
Strand-1 (RNA)⊢ [Non-Terminal Residues] ⊣Strand-1 (RNA)
Residue-6
Residue-11
Residue-7
Residue-12
Residue-8
Residue-13
Residue-9
Residue-14
Residue-10
Residue-15

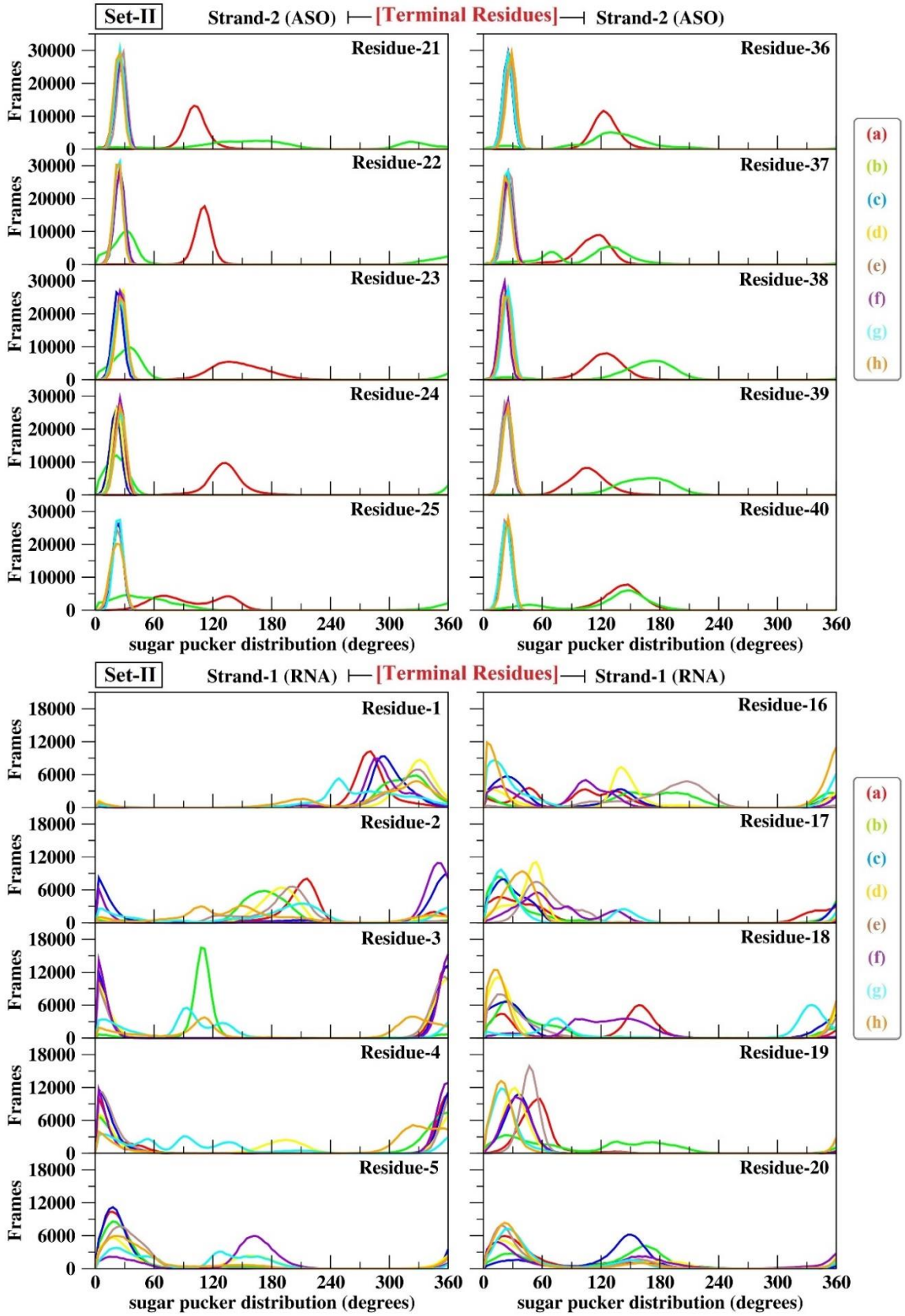
Set-II
Strand-2 (ASO) ⊢ [Terminal Residues] ⊣ Strand-2 (ASO)
Residue-21
Residue-22
Residue-23
Residue-24
Residue-25
Residue-36
Residue-37
Residue-38
Residue-39
Residue-40
Frames
sugar pucker distribution (degrees)
(a)
(b)
(c)
(d)
(e)
(f)
(g)
(h)
Set-II
Strand-1 (RNA) ⊢ [Terminal Residues] ⊣ Strand-1 (RNA)
Residue-1
Residue-2
Residue-3
Residue-4
Residue-5
Residue-16
Residue-17
Residue-18
Residue-19
Residue-20
Frames
sugar pucker distribution (degrees)

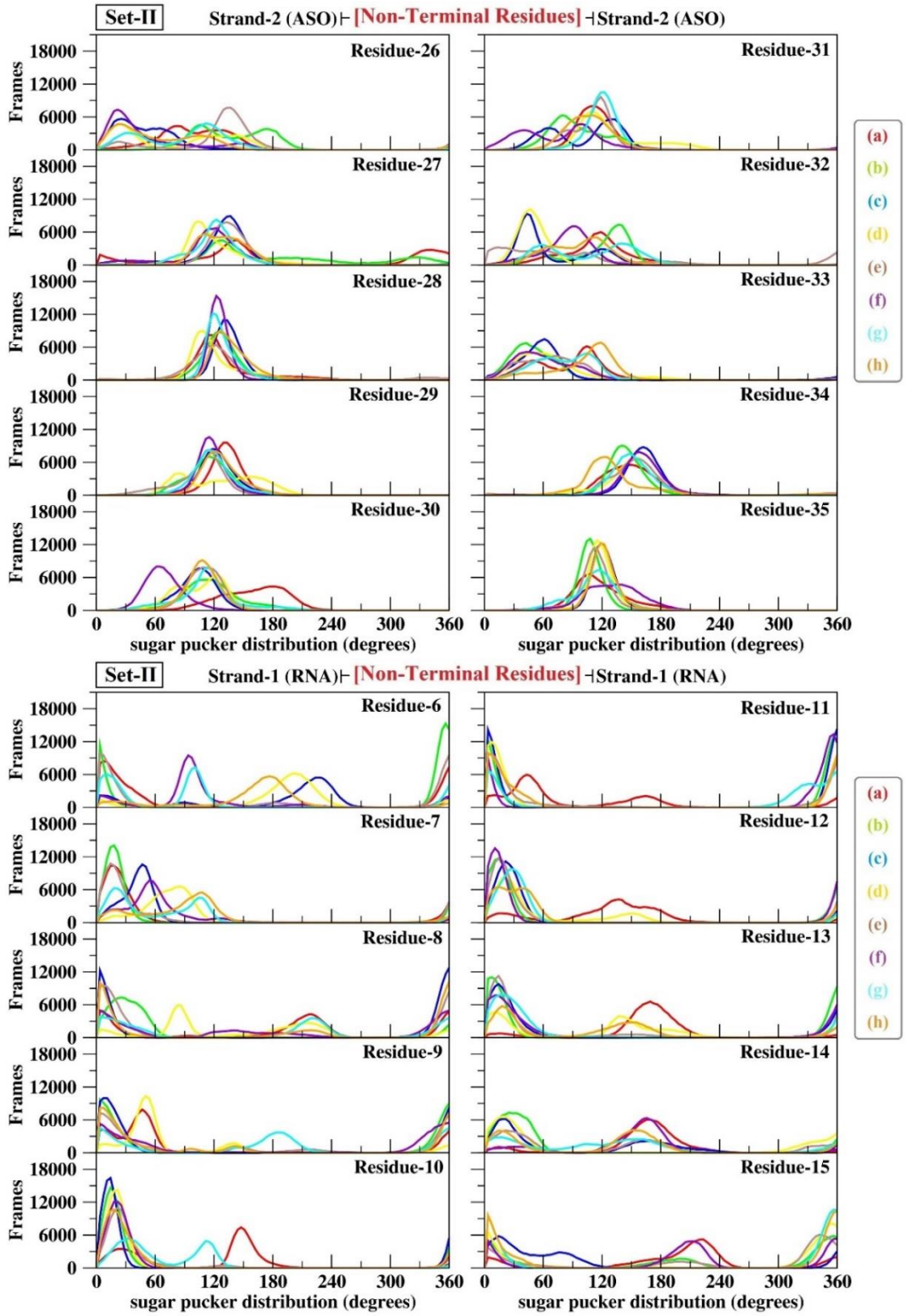

Figure 6.6: Sugar pucker distribution of the ASO/RNA duplexes (a) PS-DNA/RNA-RNaseH (b) PS-MOE/RNA-RNaseH (c) PS-LNA/RNA-RNaseH (d) PS-A1/RNA-RNaseH (e) PS-A2/RNA-RNaseH (f) PS-A3/RNA-RNaseH (g) PS-A4/RNA-RNaseH and (h) PS-A5/RNA-RNaseH of simulation trajectories from two data sets [Set-I & Set-II] each simulated for 1 μs simulation time.

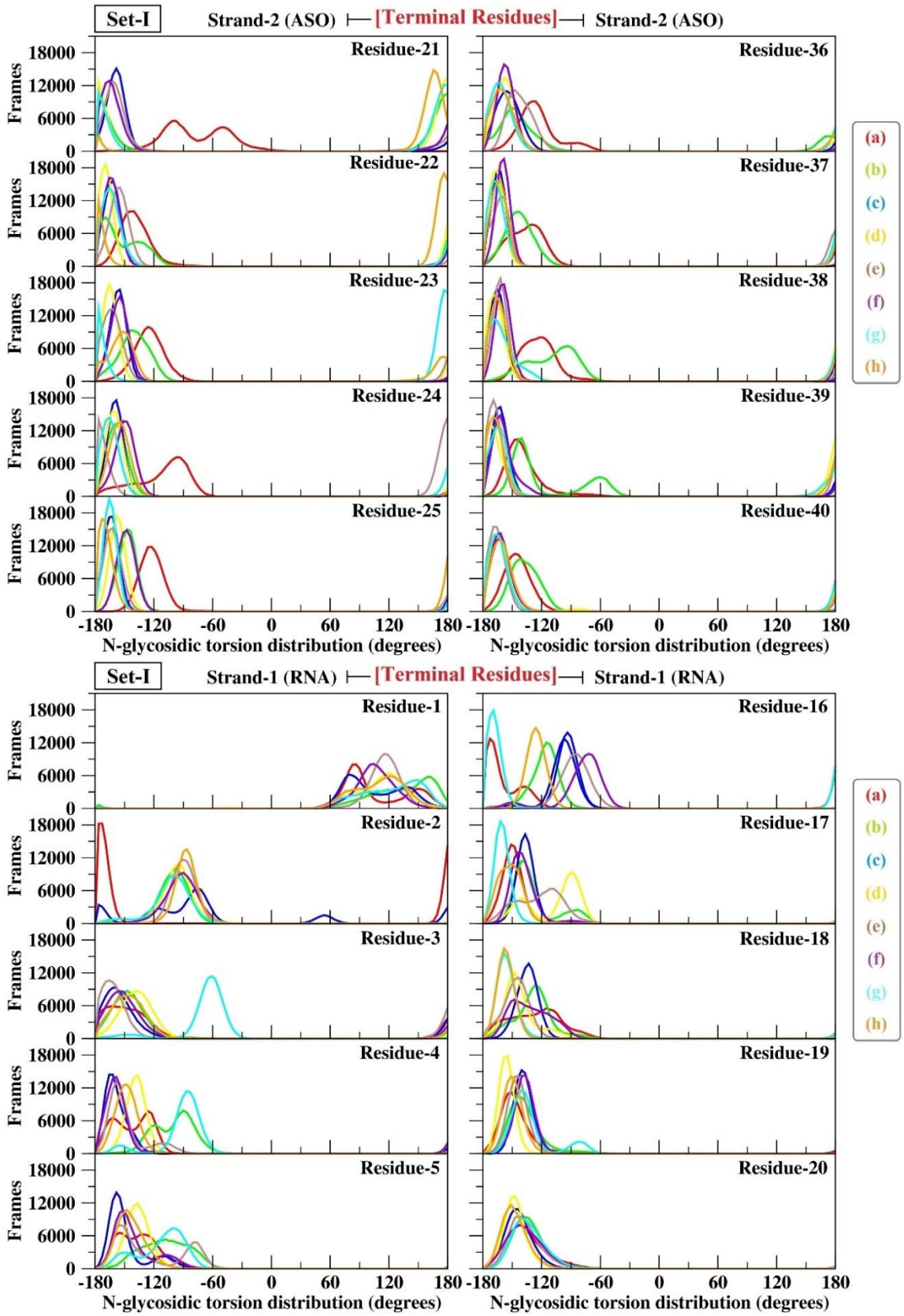
Set-I
Strand-2 (ASO) ⊢ [Terminal Residues] ⊣ Strand-2 (ASO)
Residue-21
Residue-22
Residue-23
Residue-24
Residue-25
Residue-36
Residue-37
Residue-38
Residue-39
Residue-40
Frames
18000
12000
6000
0
-180
-120
-60
0
60
120
180
N-glycosidic torsion distribution (degrees)
(a)
(b)
(c)
(d)
(e)
(f)
(g)
(h)
Set-I
Strand-1 (RNA) ⊢ [Terminal Residues] ⊣ Strand-1 (RNA)
Residue-1
Residue-2
Residue-3
Residue-4
Residue-5
Residue-16
Residue-17
Residue-18
Residue-19
Residue-20
Frames
N-glycosidic torsion distribution (degrees)

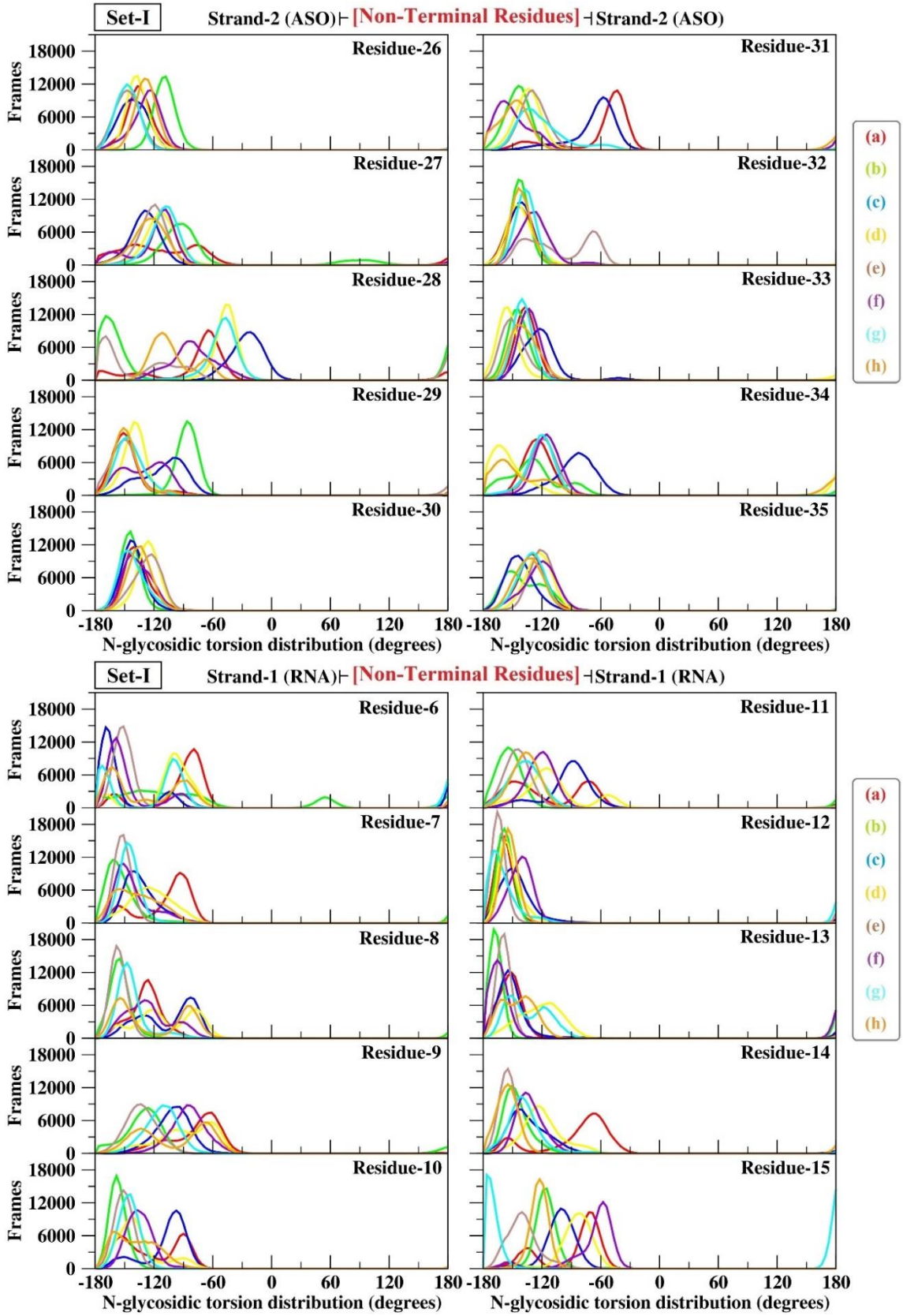
Set-I
Strand-2 (ASO)⊢ [Non-Terminal Residues] ⊣Strand-2 (ASO)
Residue-26
Residue-27
Residue-28
Residue-29
Residue-30
Residue-31
Residue-32
Residue-33
Residue-34
Residue-35
Frames
18000
12000
6000
0
-180 -120 -60 0 60 120 180
N-glycosidic torsion distribution (degrees)
(a)
(b)
(c)
(d)
(e)
(f)
(g)
(h)
Set-I
Strand-1 (RNA)⊢ [Non-Terminal Residues] ⊣Strand-1 (RNA)
Residue-6
Residue-7
Residue-8
Residue-9
Residue-10
Residue-11
Residue-12
Residue-13
Residue-14
Residue-15
Frames
18000
12000
6000
0
-180 -120 -60 0 60 120 180
N-glycosidic torsion distribution (degrees)
(a)
(b)
(c)
(d)
(e)
(f)
(g)
(h)

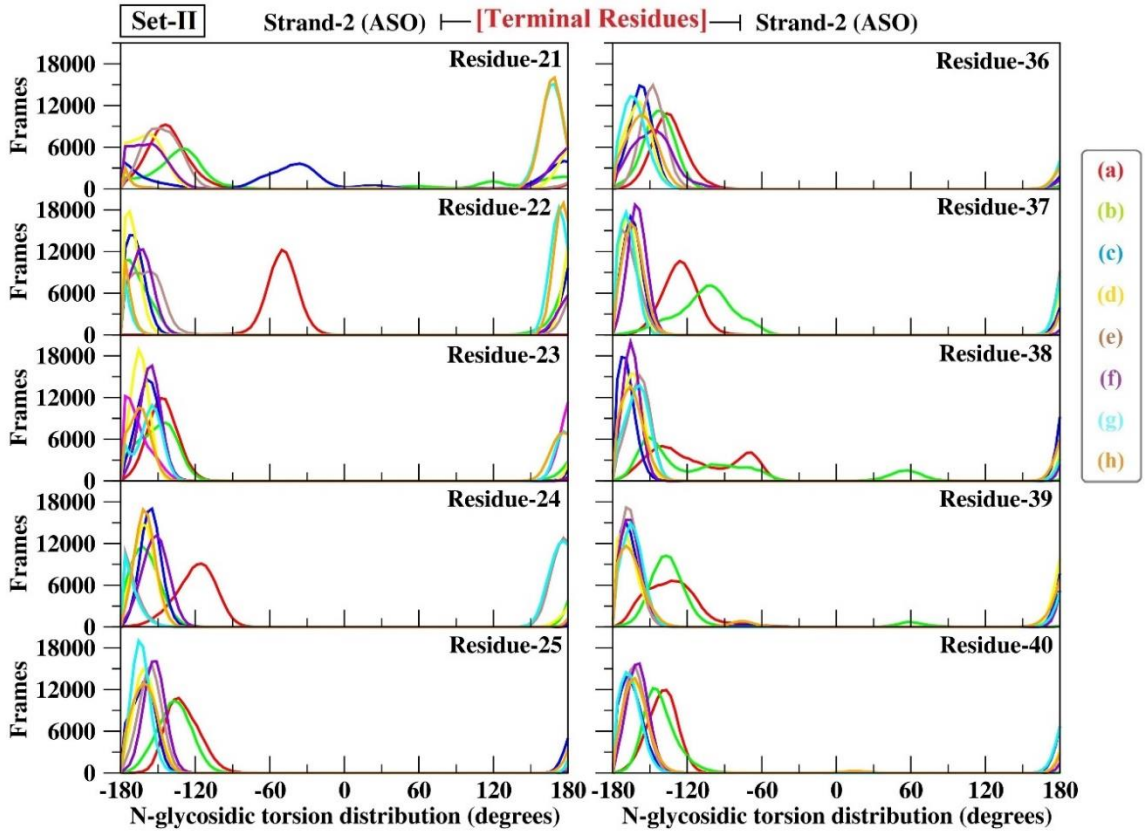
Set-II
Strand-2 (ASO) ⊢ [Terminal Residues] ⊣ Strand-2 (ASO)
Residue-21
Residue-22
Residue-23
Residue-24
Residue-25
Residue-36
Residue-37
Residue-38
Residue-39
Residue-40
Frames
18000
12000
6000
0
-180 -120 -60 0 60 120 180
N-glycosidic torsion distribution (degrees)
(a)
(b)
(c)
(d)
(e)
(f)
(g)
(h)

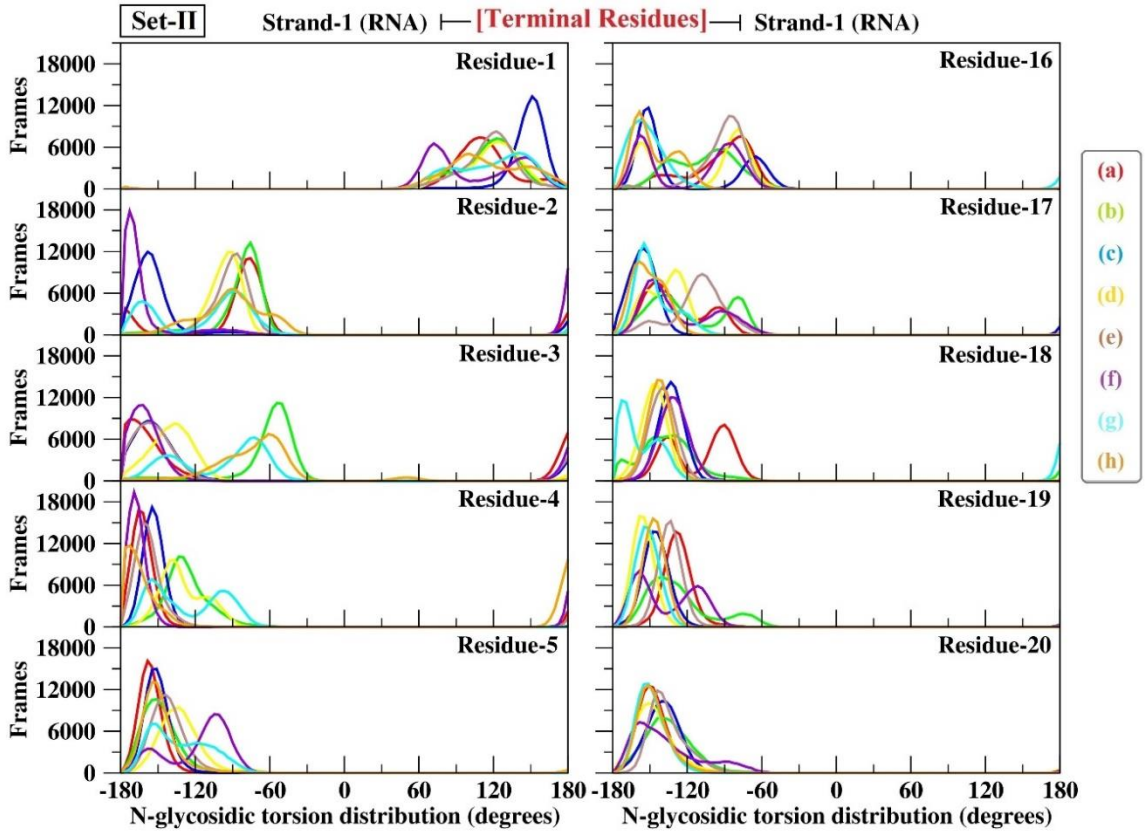
Set-II
Strand-1 (RNA) ⊢ [Terminal Residues] ⊣ Strand-1 (RNA)
Residue-1
Residue-2
Residue-3
Residue-4
Residue-5
Residue-16
Residue-17
Residue-18
Residue-19
Residue-20
Frames
18000
12000
6000
0
-180 -120 -60 0 60 120 180
N-glycosidic torsion distribution (degrees)
(a)
(b)
(c)
(d)
(e)
(f)
(g)
(h)

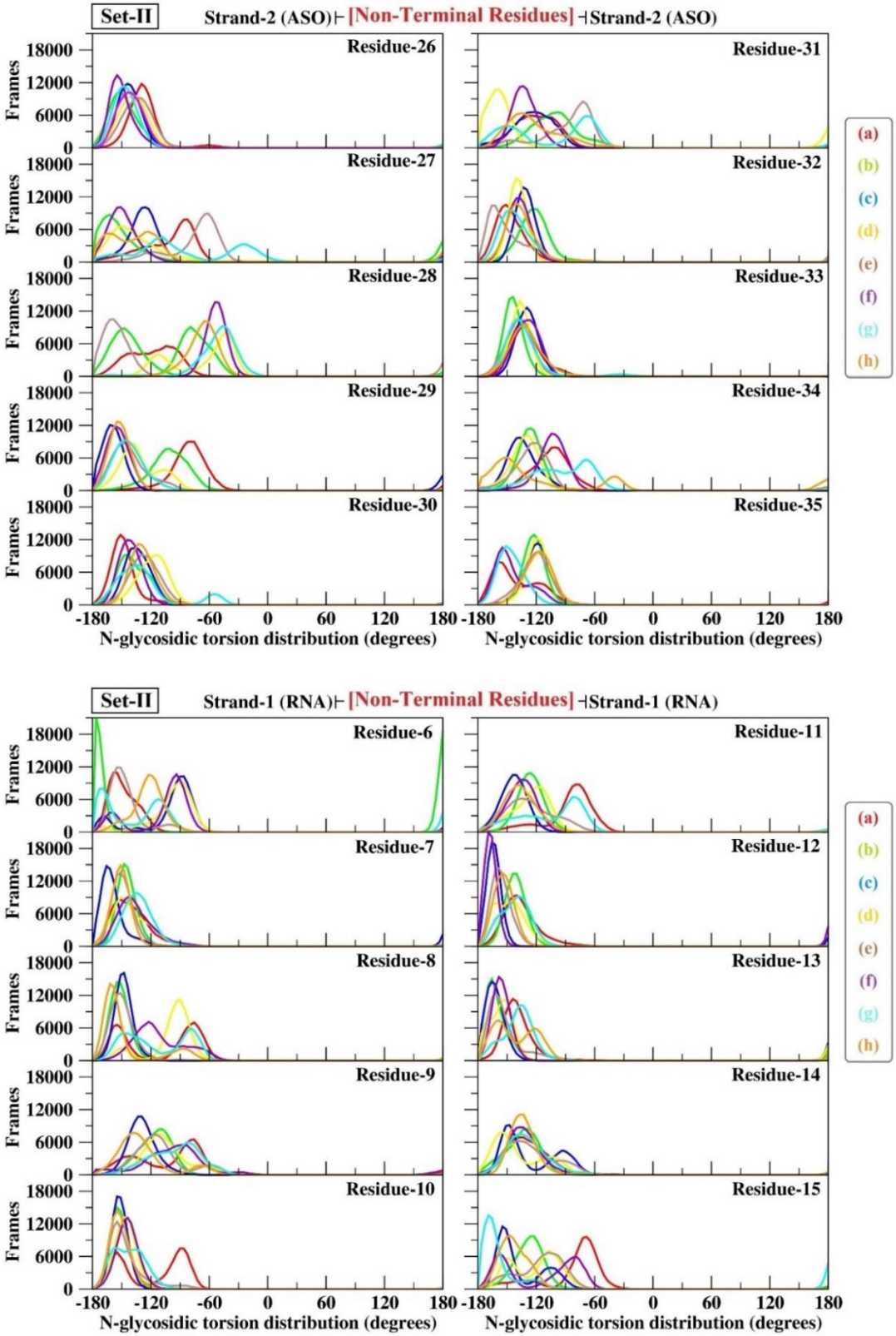

Figure 6.7: Chi distribution of the ASO/RNA duplexes (a) PS-DNA/RNA-RNaseH (b) PS-MOE/RNA-RNaseH (c) PS-LNA/RNA-RNaseH (d) PS-A1/RNA-RNaseH (e) PS-A2/RNA-RNaseH (f) PS-A3/RNA-RNaseH (g) PS-A4/RNA-RNaseH and (h) PS-A5/RNA-RNaseH of simulation trajectories from two data sets [Set-I & Set-II] each simulated for 1 µs simulation time.

6.3.5. Backbone flexibility of the modified ASO/RNA hybrid gapmer-type duplexes

To explore the influence of the duplex backbone flexibility of the ASO/RNA duplexes, residue wise RMSF of backbone heavy atoms were calculated for each nucleotide from both the nucleic acid strands, plotted in Figure 6.8. RMSF plots of the RNaseH alone are plotted in Figure 6.9. Compared to the non-terminal residues, the terminal residues typically exhibit higher flexibility, due to positional arrangement of being at the end. Accordingly, terminal residues of the duplexes demonstrated high fluctuations compared to the non-terminal residues. Detailed analysis of the fluctuations revealed that non-terminal residues of the modified systems however exhibited different fluctuations for different sets. Of all the duplexes, the PS-MOE/RNA showed highest fluctuations in set-I and PS-A4/RNA showed highest fluctuations in set-II. The PS-A5 ASO modified strand is exhibiting lowest fluctuations in set-I and PS-A5 ASO modified strand is exhibiting lowest fluctuations in set-II for the entire simulation time.

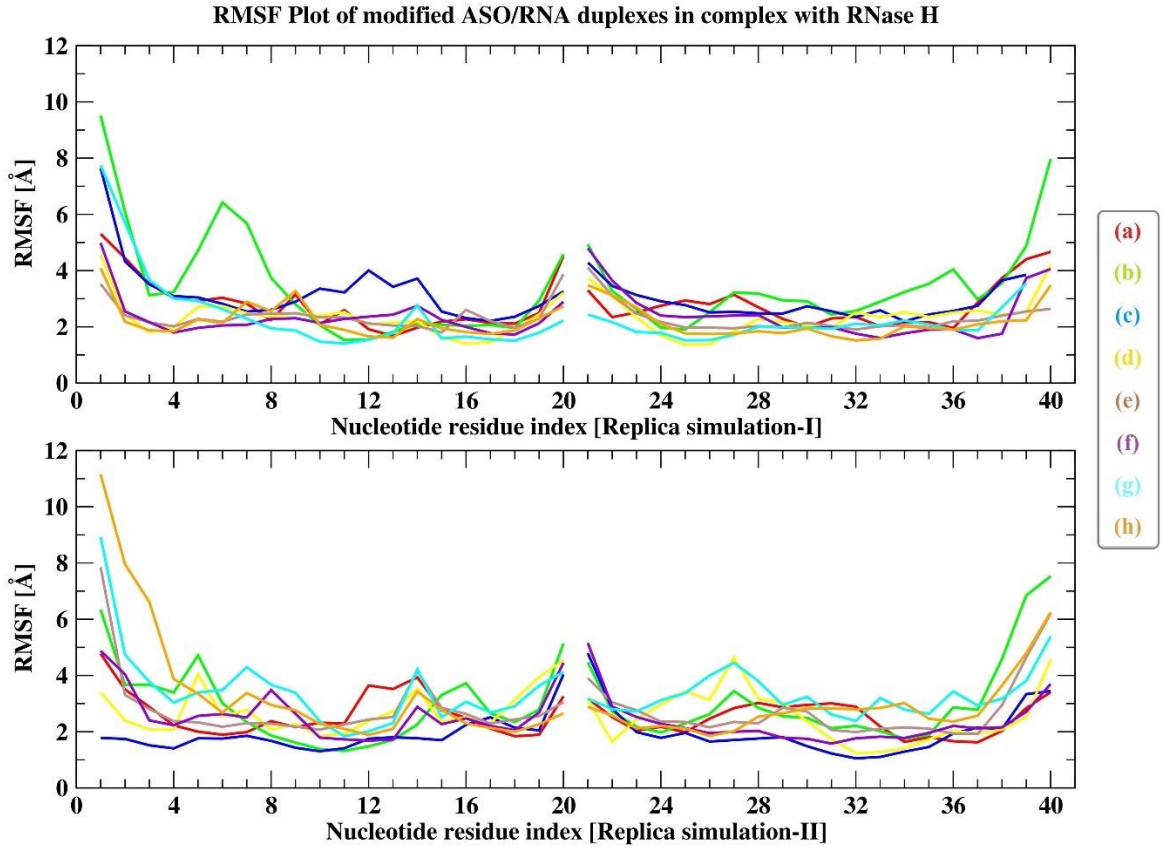

Figure 6.8: RMSF plot of ASO/RNA duplexes (a) PS-DNA/RNA-RNaseH (b) PS-MOE/RNA-RNaseH (c) PS-LNA/RNA-RNaseH (d) PS-A1/RNA-RNaseH (e) PS-A2/RNA-RNaseH (f) PS-A3/RNA-RNaseH (g) PS-A4/RNA-RNaseH and (h) PS-A5/RNA-RNaseH of simulation trajectories from two data sets [Set-I & Set-II] each simulated for 1 μs simulation time.

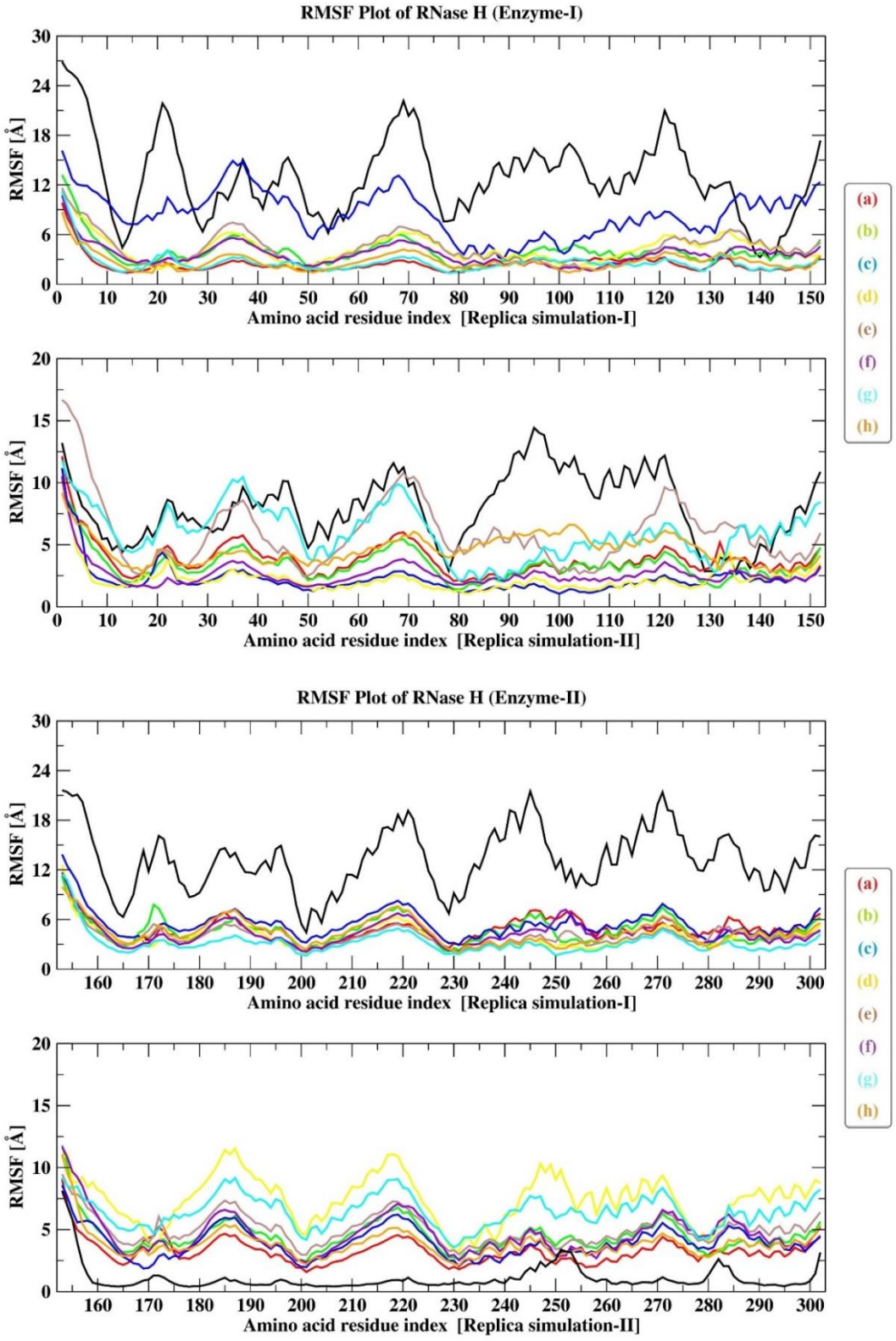

Figure 6.9: RMSF plots of the ASO/RNA duplexes (a) PS-DNA/RNA-RNaseH (b) PS-MOE/RNA-RNaseH (c) PS-LNA/RNA-RNaseH (d) PS-A1/RNA-RNaseH (e) PS-A2/RNA-RNaseH (f) PS-A3/RNA-RNaseH (g) PS-A4/RNA-RNaseH and (h) PS-A5/RNA-RNaseH of simulation trajectories from two data sets [Set-I & Set-II] each simulated for 1 μs simulation time.

6.3.6. H-Bond interactions, Base-pairing, Base-stacking and Helix-turning of the modified ASO/RNA hybrid gapmer-type duplexes

The acceptor-donor residues, average bond distances, average bond angles, bond residence frames for the complexes (a)-(h) with HBond interactions > 50 % occupancies from the simulation trajectories from both the data sets [Set-I & Set-II] were studied. H-Bond parameters of duplexes are in well agreement with the crystal data values corresponding to the *A*-form or the *B*-form conformation [65]. Amino acid residues forming HBond interactions for more than 50% residence time has been sorted and plotted in Table 6.2 which includes some common amino acid residues as ASN-19, ARG-47, TRP-93, SER-101, ILE-107, TRP-243, SER-251 at the active site of RNase H found to have interacted with all the modified ASO/RNA duplexes. Thus, apart from the aspartate and glutamate amino residues the same amino acid residues ASN-19, ARG-47, TRP-93, SER-101, ILE-107, TRP-243, SER-251 are stabilising the ASO/RNA duplexes at the active site of the RNase H.

Table 6.2: Participating residues of the ASO/RNA duplexes (a) PS-DNA/RNA-RNaseH (b) PS-MOE/RNA-RNaseH (c) PS-LNA/RNA-RNaseH (d) PS-A1/RNA-RNaseH (e) PS-A2/RNA-RNaseH (f) PS-A3/RNA-RNaseH (g) PS-A4/RNA-RNaseH and (h) PS-A5/RNA-RNaseH with HBond interactions > 50 % occupancies of simulation trajectories from two data sets [Set-I & Set-II] each simulated for 1 μs simulation time.

ASO/RNA-RNaseH Systems	Acceptor Residues	Donor Residues
(a) PS-DNA/RNA-RNaseH	U_320, TDS_327, CDS_328, GDS_336	TRP_93, SER_101, ARG_197, SER_229, SER_251
(b) PS-MOE/RNA-RNaseH	ASN_19, A_313, C_314, C_315, U_316, U_319, C_321, C3_322, MOG_324, MOA_326, MOT_327, CDS_328, ADS_329, TDS_334, CDS_335, GDS_336	ASN_19, ARG_21, ARG_47, THR_49, TRP_93, SER_101, ASN_108, GLY_131, ARG_143, ARG_146, ARG_197, GLN_201, ASN_228, TRP_243, THR_250, SER_251, ARG_296, GDS_331
(c) PS-LNA/RNA-RNaseH	GLU_204, G_304, U_320, LSG_324, CDS_328, ADS_329, TDS_334, CDS_335, GDS_336	ARG_23, ARG_47, THR_49, TRP_93, SER_101, GLU_105, ASN_108, ASN_200, MET_230, TRP_243, THR_250, SER_251, HIE_278, U_320

(d) PS-A1/RNA-RNaseH	ASN_170, ASN_200, GLU_204, A_313, C_315, U_316, U_320, C_321, C3_322, A1G_324, A1T_327, TDS_332, TDS_334, CDS_335, GDS_336	SER_17, ASN_19, ARG_21, THR_49, GLN_51, TRP_93, SER_101, ILE_107, GLY_131, ASN_170, ARG_171, ARG_172, ARG_197, ASN_200, ASN_258, U_320, A1A_325, A1A_326
(e) PS-A2/RNA-RNaseH	U_316, U_320, A2T_327, CDS_328, ADS_329, GDS_331, TDS_332, GDS_336	SER_17, ARG_21, TRP_93, SER_101, ARG_197, TRP_243, SER_251, ASN_200
(f) PS-A3/RNA-RNaseH	CYS_16, A_313, C_314, C_315, U_316, U_320, CDS_328, GDS_331, TDS_332, TDS_334, CDS_335, GDS_336	SER_17, SER_18, ASN_19, ARG_21, THR_49, TRP_93, SER_101, ILE_107, ARG_146, GLN_201, SER_251, C_314
(g) PS-A4/RNA-RNaseH	C_312, U_316, C_321, C3_322, A4G_324, A4T_327, ADS_329, TDS_334, GDS_336	SER_17, THR_49, ASN_78, TRP_93, SER_101, ARG_146, ARG_197, THR_199, ASN_228, TRP_243, SER_251, ARG_296
(h) PS-A5/RNA-RNaseH	GLU_204, C_314, C_315, U_316, U_320, C3_322, ADS_329, GDS_330, GDS_331, TDS_334, GDS_336	SER_17, ASN_19, ARG_21, ARG_47, THR_49, TRP_93, SER_101, ASN_200, TRP_243, SER_251, GLY_281, ARG_296, U_320

6.3.7. SASA of the modified ASO/RNA hybrid gapmer-type duplexes

Solvent accessible surface area (SASA) and MM-GBSA binding free energy have long been acknowledged in research on drug-protein stability and protein folding as essential components to comprehend the underlying chemistry between two molecules [66]. The SASA value represents the surface area of the ASO and RNA that is accessible to the surrounding solvent, which can give insights into the extent of interaction between the molecules and their environment. From SASA, one can analyse the changes in surface area upon duplex formation, which can indicate the binding strength and stability of the ASO/RNA complex. SASA can thus provide insights into the structural dynamics of the ASO/RNA complex, such as the degree of hydration and solvent accessibility of specific regions, which can further inform drug design strategies. Results of SASA values in Table 6.3 revealed that for the particular nucleic acid sequence were solvation of the modified ASO/RNA duplexes in presence of the RNase H was similar as the standard

antisense modifications PS-DNA, PS-MOE and PS-LNA for both Set-I & Set-II simulation trajectories. This implies that the modified ASO/RNA duplexes were very much accessible to the nearby environment for various electron-exchange activities, which may have facilitated their interaction with RNase H and the solvent environment, affecting their antisense activity.

Table 6.3: SASA of the ASO/RNA duplexes (a) PS-DNA/RNA-RNaseH (b) PS-MOE/RNA-RNaseH (c) PS-LNA/RNA-RNaseH (d) PS-A1/RNA-RNaseH (e) PS-A2/RNA-RNaseH (f) PS-A3/RNA-RNaseH (g) PS-A4/RNA-RNaseH and (h) PS-A5/RNA-RNaseH of simulation trajectories from two data sets [Set-I & Set-II] each simulated for 1 μs simulation time.

Name Code	Replica Simulation-I		Replica Simulation-II	
	$SASA_{(ASO/RNA)}$	$SASA_{RNaseH}$	$SASA_{(ASO/RNA)}$	$SASA_{RNaseH}$
(a) PS-DNA/RNA-RNaseH	13899.65	5410.04	14061.40	5849.41
(b) PS-MOE/RNA-RNaseH	13648.24	5838.37	13581.98	5725.78
(c) PS-LNA/RNA-RNaseH	14312.44	5848.45	13425.76	5511.67
(d) PS-A1/RNA-RNaseH	13750.03	5467.51	13289.56	5321.99
(e) PS-A2/RNA-RNaseH	14261.80	6230.74	14289.00	6155.82
(f) PS-A3/RNA-RNaseH	13393.93	6127.22	13937.32	6139.20
(g) PS-A4/RNA-RNaseH	13577.66	5861.09	13699.49	6176.52
(h) PS-A5/RNA-RNaseH	13566.76	5909.71	14029.14	6060.40

6.4. Summary

Simulations were conducted to study the structure and dynamic properties of a set of 20-mer ASO/RNA hybrid gapmer-type duplexes complexed with a Human RNase H catalytic domain, implementing five novel LNA-analogue antisense modifications with respect to well established LNA, MOE antisense modifications. Replica sets of MD simulations accounting to two data sets (Set-I & Set-II) were performed, each simulated for 1 μs simulation time. Stability of the duplexes throughout the simulation trajectories were studied by observing their RMSD plots. The duplexes were fluctuating potentially within and around a range of 2 to 6 Å RMSD values. The PS-MOE/RNA exhibited higher RMSD compared to the rest of the duplexes. RMSD data over time for the modified ASO/RNA duplexes showed that duplex stability is well retained for the full simulation trajectory for both sets of simulation.

Structures of the ASO/RNA gapmer-type duplexes were maintaining stable *Watson-Crick* base-pairing, base-stacking pattern and ideal helix-turning for both the sets of simulation. Base pairing is crucial for the creation of functional RNAs because it helps to maintain the folded structure of the RNA molecules by utilizing the 2′-OH group of the ribose sugar ring in base pairing interactions [67-68]. Since the LNA-based alterations are 2′-OH based modifications, this will have an impact on the modified ASO/RNA duplexes active base pairing conformations. The changed monomer nucleotides should create effective base pairing with the RNA nucleotides in order to bind sequence precisely to their target RNAs. For this to happen, the same should exist in an anti-conformation, a feature of the *A-form* helix typically observed in RNAs [69]. Additionally, the changed nucleotides in contact with the RNAs should cause the RNA nucleotides to adopt or maintain an *N-type* conformation that favors *C3′-endo* sugar puckering, reducing the ribose sugar's conformational flexibility and boosting local phosphate backbone organization. Base pairing, base stacking, and helix turning are thus closely tied to the distribution of nucleotides sugar puckers, and consequently to how the phosphate backbone is oriented in relation to either the sugar or the nucleobases.

In case of inter and intra-strand distances, residues are seen to fluctuate more for the modified ASO/RNA gapmer duplexes although no residue exhibited intra-strand distance >7 Å. Because these are hybrid duplexes, residues are seen to fluctuate more. Possible reasons suggest duplexes were adjusting highly within the RNase H catalytic domain. As such, inter-strand distances of the modified ASO/RNA duplexes were also varying compared to the wild type duplexes which are lying in the acceptable range of 19-20 Å, for both the sets of simulations. For the sugar puckering, the PS-DNA and PS-MOE contained ASOs are exhibiting *C2′-endo* conformation for the terminal residues and for the LNA and LNA-based contained ASOs, terminal residues from either end of the ASO strand are exhibiting *C3′-endo* conformation. PS-DNA modified non-terminal residues from the ASO strand are exhibiting *C2′-endo* conformation. On the other hand, the RNA strand residues are influenced by their complementary ASO strand residues. Compared to the RNA strand of the wild type duplexes, the RNA strand residues of the modified ASO/RNA duplexes although majority were exhibiting *C3′-endo* conformation, few are seen to fluctuate from the ideal *C3′-endo* conformation exhibiting a in between *C3′-endo* and the *C2′-endo* conformations.

The effect of changes on the distance between atoms immediately linked to the C1′ carbon that forms the glycosidic bond with RNA is measured by the N-glycosidic dihedral angle. The N-glycosidic bond and the accompanying chi (χ) torsion angle show that the sugar and nucleobase are two distinct objects with an internal degree of freedom. Despite having the ability to take on a wide variety of values, structural limitations restrict the values that chi (χ) can take on for clearly stated preferences. Because of the steric conflict between the nucleobase and the H3′ atom, which is directed towards the base in this specific pucker mode, *syn* glycosidic angles are unusual in nucleotides with C3′-endo sugar puckers. The stiffness and reliance of each changed nucleotide on the sugar-nucleobase orientation so that the modified nucleotides reside in an anti-conformation were investigated using the N-glycosidic dihedral angle chi (χ). In case of the modified ASO/RNA duplexes their relative sugar-base orientations were attempted to maintain anti-conformation throughout the simulation, despite residues from the ASO strands containing were influencing the N-glycosidic torsion distribution on their complementary RNA strands.

RNase H identification of antisense duplexes is greatly influenced by the flexibility of the sugar-phosphate backbone. An RNA-binding groove and a spatially conserved phosphate-binding pocket that defines a DNA-binding site make up the enzyme's active site. The minor groove width of the DNA/RNA duplexes at the phosphate binding pocket of the DNA-binding channel varies depending on the backbone's flexibility [70]. When it comes to modified ASO/RNA duplexes, backbone flexibility thus plays a key role in imparting dominant antisense activity. Compared to the non-terminal residues, terminal residues of the duplexes demonstrated high fluctuations and similar pattern of flexibility for both modified as well as the wild type duplexes. The specific van der Waals contacts and H-bond interactions at the active site of RNase H are crucial for the binding of the DNA/RNA duplexes because they allow for close fitting and surface complementarity of the sugar-phosphate backbone of the DNA. Common amino acid residues ASN-19, ARG-47, TRP-93, SER-101, ILE-107, TRP-243, and SER-251 located at the active site of RNase H were found to interact with both the wild-type and modified ASO/RNA gapmer duplexes.

Because SASA and MM-GBSA binding free energy have long been acknowledged as essential elements to comprehend the underlying chemistry in research

on protein folding and drug-protein stability, therefore will help us better comprehend the solvation pattern including the stability of the duplexes. It has been discussed already that surface area of contact between the duplexes and the water molecules increases as the SASA values increase, demonstrating that duplexes are more soluble in water. For the particular nucleic acid sequence, solvation of the modified ASO/RNA duplexes in presence of the RNase H was similar as the standard antisense modifications MOE and LNA. This suggests that the duplexes were highly accessible to the adjacent solvent environment following engagement with the RNase H, which may have affected their ability to bind to the solvent environment and possibly caused a rise in SASA values after complexation, affecting their antisense activity. In the RNase H dependent mechanism of antisense activity, RNase H is activated by the ASO/RNA duplex which specifically cleaves the RNA strand from the ASO/RNA duplex. Thus, it is expected of the RNA/DNA duplex to be more stable at the active site of RNase H. MM-GBSA binding energies of the wild type duplexes estimated for the entire simulation trajectory predicted RNA/DNA duplex to have higher affinity or is more stable at the active site of the RNase H catalytic domain. Given that DNA homo duplexes are less stable compared to RNA homo duplexes and RNA/DNA hybrid duplexes in nature it was observed that free energy of RNA/RNA is highest and DNA/DNA is lowest with RNA/DNA being the intermediate. In case of modified ASO/RNA duplexes, free energy of binding was highest for the PS-MOE/RNA-RNaseH system, for both simulation trajectories. MM-GBSA binding energies estimated for the entire simulation trajectory predicted rest of the modifications to have comparable ΔG values with the PS-MOE modifications.

Bibliography

[1] Dias, N., and Stein, C. A. Antisense oligonucleotides: basic concepts and mechanisms. *Molecular cancer therapeutics, 1*(5):347-355, 2002.

[2] Kurreck, J. Antisense technologies: improvement through novel chemical modifications. *European journal of biochemistry*, *270*(8): 1628-1644, 2003.

[3] Le Calvez, H., Yu, M., and Fang, F. Biochemical prevention and treatment of viral infections–A new paradigm in medicine for infectious diseases. *Virology Journal*, *1*:1-6. 2004.

[4] Takei, Y., Kadomatsu, K., Yuzawa, Y., Matsuo, S., and Muramatsu, T. A small interfering RNA targeting vascular endothelial growth factor as cancer therapeutics. *Cancer research*, *64*(10): 3365-3370, 2004.

[5] Gong, M., Lu, Z., Fang, G., Bi, J., and Xue, X. A small interfering RNA targeting osteopontin as gastric cancer therapeutics. *Cancer letters*, *272*(1):148-159, 2008.

[6] Stein, C. A., and Castanotto, D. FDA-approved oligonucleotide therapies in 2017. *Molecular Therapy*, *25*(5): 1069-1075, 2017.

[7] Silva, A. C., Lobo, D. D., Martins, I. M., Lopes, S. M., Henriques, C., Duarte, S. P., ... and Pereira de Almeida, L. Antisense oligonucleotide therapeutics in neurodegenerative diseases: the case of polyglutamine disorders. *Brain*, *143*(2): 407-429, 2020.

[8] Chan, J. H., Lim, S., and Wong, W. F. Antisense oligonucleotides: from design to therapeutic application. *Clinical and experimental pharmacology and physiology*, *33*(5-6): 533-540, 2006.

[9] Bennett, C. F., and Swayze, E. E. RNA targeting therapeutics: molecular mechanisms of antisense oligonucleotides as a therapeutic platform. *Annual review of pharmacology and toxicology*, *50*: 259-293, 2010.

[10] Moss, K. H., Popova, P., Hadrup, S. R., Astakhova, K., and Taskova, M. Lipid nanoparticles for delivery of therapeutic RNA oligonucleotides. *Molecular pharmaceutics*, *16*(6): 2265-2277, 2019.

[11] Gheibi-Hayat, S. M., and Jamialahmadi, K. Antisense Oligonucleotide (AS-ODN) Technology: Principle, Mechanism and Challenges. *Biotechnology and Applied Biochemistry*, *68*(5): 1086-1094, 2021.

[12] Zamaratski, E., Pradeepkumar, P. I., and Chattopadhyaya, J. A critical survey of the structure-function of the antisense oligo/RNA heteroduplex as substrate for RNase H. *Journal of biochemical and biophysical methods*, *48*(3): 189-208. 2001.

[13] Nowotny, M., Gaidamakov, S. A., Ghirlando, R., Cerritelli, S. M., Crouch, R. J., and Yang, W. Structure of human RNase H1 complexed with an RNA/DNA hybrid: insight into HIV reverse transcription. *Molecular cell*, *28*(2): 264-276. 2007.

[14] Kiełpiński, Ł. J., Hagedorn, P. H., Lindow, M., and Vinther, J. RNase H sequence preferences influence antisense oligonucleotide efficiency. *Nucleic acids research*, *45*(22): 12932-12944, 2017.

[15] Hagedorn, P. H., Pontoppidan, M., Bisgaard, T. S., Berrera, M., Dieckmann, A., Ebeling, M., ... and Lindow, M. Identifying and avoiding off-target effects of RNase H-dependent antisense oligonucleotides in mice. *Nucleic Acids Research*, *46*(11): 5366-5380, 2018.

[16] Herbert, C., Dzowo, Y. K., Urban, A., Kiggins, C. N., and Resendiz, M. J. Reactivity and specificity of RNase T1, RNase A, and RNase H toward oligonucleotides of RNA containing 8-Oxo-7, 8-dihydroguanosine. *Biochemistry*, *57*(20): 2971-2983, 2018.

[17] Zamecnik, P. C., and Stephenson, M. L. Inhibition of Rous sarcoma virus replication and cell transformation by a specific oligodeoxynucleotide. *Proceedings of the National Academy of Sciences*, *75*(1): 280-284, 1978.

[18] Campbell, J. M., Bacon, T. A., and Wickstrom, E. Oligodeoxynucleoside phosphorothioate stability in subcellular extracts, culture media, sera and cerebrospinal fluid. *Journal of biochemical and biophysical methods*, *20*(3): 259-267, 1990.

[19] Zhang, R., Diasio, R. B., Lu, Z., Liu, T., Jiang, Z., Galbraith, W. M., and Agrawal, S. Pharmacokinetics and tissue distribution in rats of an oligodeoxynucleotide phosphorothioate (GEM 91) developed as a therapeutic agent for human immunodeficiency virus type-1. *Biochemical pharmacology*, *49*(7): 929-939, 1995.

[20] Agrawal, S., Goodchild, J., Civeira, M., Sarin, P. S., and Zamecnik, P. C. Phosphoramidate, phosphorothioate, and methylphosphonateanalogs of oligodeoxynucleotide: inhibitors of replication of human immunodeficiency virus. *Nucleosides & Nucleotides*, *8*(5-6): 819-823, (1989).

[21] Iwamoto, N., Butler, D. C., Svrzikapa, N., Mohapatra, S., Zlatev, I., Sah, D. W., ... and Verdine, G. L. Control of phosphorothioate stereochemistry substantially increases the efficacy of antisense oligonucleotides. *Nature biotechnology*, *35*(9): 845-851, 2017.

[22] Shen, W., De Hoyos, C. L., Migawa, M. T., Vickers, T. A., Sun, H., Low, A., ... and Crooke, S. T. Chemical modification of PS-ASO therapeutics reduces cellular protein-binding and improves the therapeutic index. *Nature biotechnology*, *37*(6): 640-650, 2019.

[23] Vitravene Study Group. A randomized controlled clinical trial of intravitreous fomivirsen for treatment of newly diagnosed peripheral cytomegalovirus retinitis in patients with AIDS. *American Journal of Ophthalmology*, *133*(4): 467-474, 2002.

[24] Manoharan, M. 2′-Carbohydrate modifications in antisense oligonucleotide therapy: importance of conformation, configuration and conjugation. *Biochimica et Biophysica Acta (BBA)-Gene Structure and Expression*, *1489*(1): 117-130, 1999.

[25] Herdewijn, P. Conformationally restricted carbohydrate-modified nucleic acids and antisense technology. *Biochimica et Biophysica Acta (BBA)-Gene Structure and Expression*, *1489*(1):167-179, 1999.

[26] Rosie, Z. Y., Kim, T. W., Hong, A., Watanabe, T. A., Gaus, H. J., and Geary, R. S. Cross-species pharmacokinetic comparison from mouse to man of a second-generation antisense oligonucleotide, ISIS 301012, targeting human apolipoprotein B-100. *Drug Metabolism and Disposition*, *35*(3): 460-468, 2007.

[27] Geary, R. S., Wancewicz, E., Matson, J., Pearce, M., Siwkowski, A., Swayze, E., and Bennett, F. Effect of dose and plasma concentration on liver uptake and pharmacologic activity of a 2′-methoxyethyl modified chimeric antisense oligonucleotide targeting PTEN. *Biochemical pharmacology*, *78*(3): 284-291. 2009.

[28] Advani, P. P., Paulus, A., Masood, A., Sher, T., and Chanan-Khan, A. Pharmacokinetic evaluation of oblimersen sodium for the treatment of chronic lymphocytic leukemia. *Expert opinion on drug metabolism & toxicology*, *7*(6): 765-774, 2011.

[29] Aartsma-Rus, A. FDA approval of nusinersen for spinal muscular atrophy makes 2016 the year of splice modulating oligonucleotides. *Nucleic acid therapeutics*, *27*(2): 67-69, 2017.

[30] Aartsma-Rus, A., and Krieg, A. M. FDA approves eteplirsen for Duchenne muscular dystrophy: the next chapter in the eteplirsen saga. *Nucleic acid therapeutics*, *27*(1): 1-3, 2017.

[31] Singh, S. K., Koshkin, A. A., Wengel, J., and Nielsen, P. LNA (locked nucleic acids): synthesis and high-affinity nucleic acid recognition. *Chemical communications*, (4): 455-456, 1998.

[32] Abdur Rahman, S. M., Seki, S., Obika, S., Yoshikawa, H., Miyashita, K., and Imanishi, T. Design, synthesis, and properties of 2 ‘, 4 ‘-BNA^{NC}: a bridged nucleic acid analogue. *Journal of the american chemical society*, *130*(14): 4886-4896, 2008.

[33] Shrestha, A. R., Kotobuki, Y., Hari, Y., and Obika, S. Guanidine bridged nucleic acid (GuNA): an effect of a cationic bridged nucleic acid on DNA binding affinity. *Chemical Communications*, *50*(5): 575-577, 2014.

[34] Langner, H. K., Jastrzebska, K., and Caruthers, M. H. Synthesis and characterization of thiophosphoramidate morpholino oligonucleotides and chimeras. *Journal of the American Chemical Society*, *142*(38): 16240-16253, 2020.

[35] Fluiter, K., ten Asbroek, A. L., de Wissel, M. B., Jakobs, M. E., Wissenbach, M., Olsson, H., ... and Baas, F. In vivo tumor growth inhibition and biodistribution studies of locked nucleic acid (LNA) antisense oligonucleotides. *Nucleic acids research*, *31*(3): 953-962, 2003.

[36] Darfeuille, F., Hansen, J. B., Orum, H., Primo, C. D., and Toulmé, J. J. LNA/DNA chimeric oligomers mimic RNA aptamers targeted to the TAR RNA element of HIV-1. *Nucleic acids research*, *32*(10): 3101-3107, 2004.

[37] Laxton, C., Brady, K., Moschos, S., Turnpenny, P., Rawal, J., Pryde, D. C., ... and Murray, E. J. Selection, optimization, and pharmacokinetic properties of a novel, potent antiviral locked nucleic acid-based antisense oligomer targeting hepatitis C virus internal ribosome entry site. *Antimicrobial agents and chemotherapy*, *55*(7): 3105-3114, 2011.

[38] Swayze, E. E., Siwkowski, A. M., Wancewicz, E. V., Migawa, M. T., Wyrzykiewicz, T. K., Hung, G., ... and Bennett, A. C. F. Antisense oligonucleotides containing locked nucleic acid improve potency but cause significant hepatotoxicity in animals. *Nucleic acids research*, *35*(2): 687-700, 2007.

[39] Seth, P. P., Siwkowski, A., Allerson, C. R., Vasquez, G., Lee, S., Prakash, T. P., ... and Swayze, E. E. Short antisense oligonucleotides with novel 2′− 4′ conformationaly restricted nucleoside analogues show improved potency without increased toxicity in animals. *Journal of medicinal chemistry*, *52*(1): 10-13, 2009.

[40] Seth, P. P., Vasquez, G., Allerson, C. A., Berdeja, A., Gaus, H., Kinberger, G. A., ... and Swayze, E. E. Synthesis and biophysical evaluation of 2′, 4′-constrained 2′ O-methoxyethyl and 2′, 4′-constrained 2′ O-ethyl nucleic acid analogues. *The Journal of organic chemistry*, *75*(5): 1569-1581, 2010.

[41] Prakash, T. P., Siwkowski, A., Allerson, C. R., Migawa, M. T., Lee, S., Gaus, H. J., ... and Bhat, B. Antisense oligonucleotides containing conformationally constrained 2′, 4′-(N-methoxy) aminomethylene and 2′, 4′-aminooxymethylene and 2′-O, 4′-C-aminomethylene bridged nucleoside analogues show improved potency in animal models. *Journal of Medicinal Chemistry*, *53*(4):1636-1650, 2010.

[42] Yamamoto, T., Yasuhara, H., Wada, F., Harada-Shiba, M., Imanishi, T., and Obika, S. Superior silencing by 2′, 4′-BNA^{NC}-based short antisense oligonucleotides compared to 2′, 4′-BNA/LNA-based apolipoprotein B antisense inhibitors. *Journal of Nucleic Acids*, *2012*.

[43] Natsume, T.; Ishikawa, Y.; Dedachi, K.; Tsukamoto and T.; Kurita, N. DFT study of the electronic properties of DNA−DNA and PNA−DNA double strands. *International Journal of Quantum Chemistry*, 106: 3278−3287, 2006.

[44] Uppuladinne, M. V., Jani, V., Sonavane, U. B., and Joshi, R. R. Quantum chemical studies of novel 2′-4′ conformationally restricted antisense monomers. *International Journal of Quantum Chemistry*, *113*(23): 2523-2533, 2013.

[45] Bhai, S., and Ganguly, B. Role of backbones on the interaction of metal ions with deoxyribonucleic acid and peptide nucleic acid: A DFT study. *Journal of Molecular Graphics and Modelling*, *93*: 107445, 2019.

[46] Uppuladinne, M. V., Sonavane, U. B., Deka, R. C., and Joshi, R. R. Structural insight into antisense gapmer-RNA oligomer duplexes through molecular dynamics simulations. *Journal of Biomolecular Structure and Dynamics*, *37*(11): 2823-2836, 2019.

[47] Galindo-Murillo, R., Cohen, J. S., and Akabayov, B. Molecular dynamics simulations of acyclic analogs of nucleic acids for antisense inhibition. *Molecular Therapy-Nucleic Acids*, *23*: 527-535, 2021.

[48] Uppuladinne, M. V., Dowerah, D., Sonavane, U. B., Ray, S. K., Deka, R. C., and Joshi, R. R. Structural insight into locked nucleic acid based novel antisense modifications: A DFT calculations at monomer and MD simulations at oligomer level. *Journal of Molecular Graphics and Modelling*, *107*: 107945, 2021.

[49] Hansen, H. F., Albaek, N., Hansen, B. R., Shim, I., Bohr, H., and Koch, T. In vivo uptake of antisense oligonucleotide drugs predicted by ab initio quantum mechanical calculations. *Scientific Reports*, *11*(1): 6321, 2021.

[50] Dowerah, D., VN Uppuladinne, M., Sarma, P. J., Biswakarma, N., Sonavane, U. B., Joshi, R. R., ... and Deka, R. C. Design of LNA Analogues Using a Combined Density Functional Theory and Molecular Dynamics Approach for RNA Therapeutics. *ACS Omega*, 2023.

[51] D.A. Case, I.Y. Ben-Shalom, S.R. Brozell, D.S. Cerutti, T.E. Cheatham, III, V.W.D. Cruzeiro, T.A. Darden, R.E. Duke, D. Ghoreishi, M.K. Gilson, H. Gohlke, A.W. Goetz, D. Greene, R Harris, N. Homeyer, Y. Huang, S. Izadi, A. Kovalenko, T. Kurtzman, T.S. Lee, S. LeGrand, P. Li, C. Lin, J. Liu, T. Luchko, R. Luo, D.J. Mermelstein, K.M. Merz, Y. Miao, G. Monard, C. Nguyen, H. Nguyen, I. Omelyan, A. Onufriev, F. Pan, R. Qi, D.R. Roe, A. Roitberg, C. Sagui, S. Schott-Verdugo, J.

Shen, C.L. Simmerling, J. Smith, R. SalomonFerrer, J. Swails, R.C. Walker, J. Wang, H. Wei, R.M. Wolf, X. Wu, L. Xiao, D.M. York and P.A. Kollman. AMBER 2018, University of California, San Francisco, 2018.

[52] Frisch, M. J.; Trucks, G.W.; Schlegel, H. B.; Scuseria, G. E.; Robb, M. A.; Cheeseman, J. R.; Scalmani, G.; Barone, V.; Mennucci, B.; Petersson, G. A.; Nakatsuji, H. Gaussian 09, Revision D. 01, Gaussian, Inc., Wallingford CT, 2009.

[53] Wang, Y., Verma, P., Jin, X., Truhlar, D. G., and He, X. Revised M06 density functional for main-group and transition-metal chemistry. *Proceedings of the National Academy of Sciences*, *115*(41): 10257-10262, 2018.

[54] Jorgensen, W. L., Chandrasekhar, J., Madura, J. D., Impey, R. W., and Klein, M. L. Comparison of simple potential functions for simulating liquid water. *The Journal of chemical physics*, *79*(2): 926-935,1983.

[55] Machireddy, B., Kalra, G., Jonnalagadda, S., Ramanujachary, K., and Wu, C. Probing the binding pathway of BRACO19 to a parallel-stranded human telomeric G-quadruplex using molecular dynamics binding simulation with AMBER DNA OL15 and ligand GAFF2 force fields. *Journal of chemical information and modeling*, *57*(11): 2846-2864, 2017.

[56] Zhao, J., Kennedy, S. D., and Turner, D. H. Nuclear magnetic resonance spectra and AMBER OL3 and ROC-RNA simulations of UCUCGU reveal force field strengths and weaknesses for single-stranded RNA. *Journal of Chemical Theory and Computation*, *18*(2): 1241-1254, 2022.

[57] Cheatham, T. I., Miller, J. L., Fox, T., Darden, T. A., and Kollman, P. A. Molecular dynamics simulations on solvated biomolecular systems: the particle mesh Ewald method leads to stable trajectories of DNA, RNA, and proteins. *Journal of the American Chemical Society*, *117*(14): 4193-4194, 1995.

[58] Miyamoto, S., & Kollman, P. A. Settle: An analytical version of the SHAKE and RATTLE algorithm for rigid water models. *Journal of computational chemistry*, *13*(8): 952-962, 1992.

[59] Roe, D. R., and Cheatham III, T. E. PTRAJ and CPPTRAJ: software for processing and analysis of molecular dynamics trajectory data. *Journal of chemical theory and computation*, *9*(7): 3084-3095, 2013.

[60] Xu, L., Sun, H., Li, Y., Wang, J., and Hou, T. Assessing the performance of MM/PBSA and MM/GBSA methods. 3. The impact of force fields and ligand charge models. *The journal of physical chemistry B*, *117*(28): 8408-8421, 2013.

[61] Ho, P. S., and Carter, M. DNA structure: alphabet soup for the cellular soul. In *DNA replication-current advances*. IntechOpen, 2011.

[62] Xia, Z., Bell, D. R., Shi, Y., and Ren, P. RNA 3D structure prediction by using a coarse-grained model and experimental data. *The Journal of Physical Chemistry B*, *117*(11): 3135-3144, 2013.

[63] Hanessian, S., Schroeder, B. R., Giacometti, R. D., Merner, B. L., Østergaard, M., Swayze, E. E., and Seth, P. P. Structure-Based Design of a Highly Constrained Nucleic Acid Analogue: Improved Duplex Stabilization by Restricting Sugar Pucker and Torsion Angle γ. *AngewandteChemie International Edition*, *51*(45): 11242-11245, 2012.

[64] Heinemann, U., and Roske, Y. Symmetry in nucleic-acid double helices. *Symmetry*, *12*(5): 737, 2020.

[65] Parker, T. M., Hohenstein, E. G., Parrish, R. M., Hud, N. V., and Sherrill, C. D. Quantum-mechanical analysis of the energetic contributions to π stacking in nucleic acids versus rise, twist, and slide. *Journal of the American Chemical Society*, *135*(4): 1306-1316, 2013.

[66] Chen, F., Sun, H., Wang, J., Zhu, F., Liu, H., Wang, Z., ... and Hou, T. Assessing the performance of MM/PBSA and MM/GBSA methods. 8. Predicting binding free energies and poses of protein–RNA complexes. *Rna*, *24*(9): 1183-1194, 2018.

[67] Yakovchuk, P., Protozanova, E., and Frank-Kamenetskii, M. D. Base-stacking and base-pairing contributions into thermal stability of the DNA double helix. *Nucleic acids research*, *34*(2): 564-574, 2006.

[68] Sponer, J., Zgarbová, M., Jurecka, P., Riley, K. E., Sponer, J. E., and Hobza, P. Reference quantum chemical calculations on RNA base pairs directly involving the 2′-OH group of ribose. *Journal of Chemical Theory and Computation*, *5*(4): 1166-1179, 2009.

[69] Butcher, S. E., and Pyle, A. M. The molecular interactions that stabilize RNA tertiary structure: RNA motifs, patterns, and networks. *Accounts of chemical research*, *44*(12): 1302-1311, 2011.

[70] Noy, A., Luque, F. J., and Orozco, M. Theoretical analysis of antisense duplexes: determinants of the RNase H susceptibility. *Journal of the American Chemical Society*, *130*(11): 3486-3496, 2008.